4. RESULTS AND DISCUSSION

In the present study, antimicrobial and anti-inflammatory properties exhibited by silver and gold nanobioconjugates synthesized from the leaf extracts of *Clitoria ternatea* bearing blue and white flowers were determined in comparison with the respective unconjugated extracts. The results obtained are presented and discussed in this chapter.

PHASE I

In the first phase, leaves, seeds and roots of two varieties of *Clitoria ternatea* were examined for their antioxidant and antimicrobial activity. Extracts of different solvents of varying polarity were analyzed. The extracts were also assessed for their bioactivity namely *in vitro* antibacterial activity, in order to determine whether they elicited a biological response.

4.1 RADICAL SCAVENGING EFFECTS:

Free radical-induced oxidative damage is involved in the pathogenesis of many chronic and degenerative diseases, such as cardiovascular disease, cancer, diabetes, neurodegenerative disease and ageing. Reactive oxygen species (ROS), including superoxide free radical, hydrogen peroxide, hydroxyl free radical and singlet oxygen, play a key role in the oxidative damage of these diseases, which may result in DNA mutations, protein inactivation, lipid peroxidation, cell apoptosis or abnormal proliferation, eliciting the occurrence of diseases from the cellular and molecular levels (Rahman *et al*., 2012).

Antioxidants are substances capable of scavenging ROS and protecting from oxidative damage. Natural antioxidants, such as vitamins and polyphenols, have high antioxidant capacities and are abundant in many fruits and vegetables, whose consumption has been demonstrated to be inversely associated with the cardiovascular disease and some cancers (Kumar, 2014).

In the present study, the antioxidant potential of the extracts of different parts of *Clitoria ternatea*, prepared in solvents of varying polarity, was tested using a battery of radicals and oxidants namely DPPH, ABTS, hydroxyl and hydrogen peroxide. The results obtained are given below.

4.1.1 DPPH scavenging effects:

DPPH scavenging ability of methanol extract of the leaves, seeds and roots of the candidate plant was assessed. DPPH is a stable free radical used to evaluate the effectiveness of antioxidants (Ramachandran and Nair, 2011).

The results of the present study showed that the methanol extracts of *Clitoria ternatea* bearing blue and white flowers were very effective in scavenging DPPH radicals (Figure 4.1) compared to the extracts in other solvents. Among the different plant parts (leaves, seeds and roots) compared, leaves showed better scavenging activity than seeds and roots.

Lee *et al*. (2016) studied DPPH scavenging activity *Lespedeza bicolor* extract and its fractions, and reported that the ethyl acetate fraction has 4 times lower scavenging activity when compared to ascorbic acid. Sakat *et al*. (2010) assessed the methanolic extract of whole plant of *Oxalis corniculata* Linn. for its antioxidant activity, at different concentrations. The extract exhibited significant DPPH and nitric oxide radical scavenging activity.

Zhang *et al*. (2015) investigated the bioactive constituents of *Xanthoceras sorbifolia* for their antioxidant activity using DPPH radicals. Saxena *et al*. (2011) have reviewed different methods to assess the antioxidant activity of some common plants of Indian traditional medicine namely *Emblica officinalis* L., *Curcuma longa* L., *Mangifera indica* L., *Momordica charantia* L., *Santalum album* L., *Swertia chirata* and *Withania somnifera* (L.) for their historical, etymological, morphological, phytochemical and pharmacological aspects, and reported that these plants contain antioxidant principles that can explain and justify their use in traditional medicine in the past as well as the present.

Enechi *et al*. (2013) conducted DPPH radical-scavenging, iron (II)-chelating, NO radical-scavenging, ferrous sulphate and carbon tetra chloride induced lipid peroxidation assay of *Alternanthera brasiliana* extract and provided evidences for the natural antioxidant richness in the ethanol extract of the leaves of *A. brasiliana* and justified its use in folk medicine especially in the management of free radical-mediated disorders.

Balakrishnan *et al*. (2013) also examined the antioxidant effects and apoptotic study of different solvent extracts of *Clitoria ternatea* and *Alternanthra sessilis* leaves by DPPH dot plot rapid screening assay and DNA damage in yeast cells, and found the maximum antioxidant activity in the methanol extract followed by the ethanol extract and aqueous extract. The antioxidant properties of *C. ternatea* have been assayed using the free radical DPPH, wherein the methanolic extract showed good antioxidant activity than hexane and chloroform extracts of whole plant (Madhavarao *et al*., 2011).

In our study also, the methanolic extracts of the leaves showed higher DPPH scavenging effect than the other solvent extracts, in both the varieties of the plant.

4.1.2 ABTS scavenging effects:

The radical scavenging effect of different solvent extracts of the leaves, seeds and roots were assessed by ABTS (2,2'-azino-bis-3-ethyl benzthiazoline-6-sulphonic acid) radical cation de-colourisation assay and the results revealed that the methanol extracts of *Clitoria ternatea* bearing blue and white flowers were more effective in scavenging ABTS radicals (Figure 4.2) compared to the other solvent extracts. Among the different plant parts studied, leaf extracts showed better scavenging activity than seeds and roots in a majority of the solvents analysed.

Figure 4.1

DPPH scavenging activity of different solvent extracts of leaves, seeds and roots of *Clitoria ternatea* bearing blue and white flowers

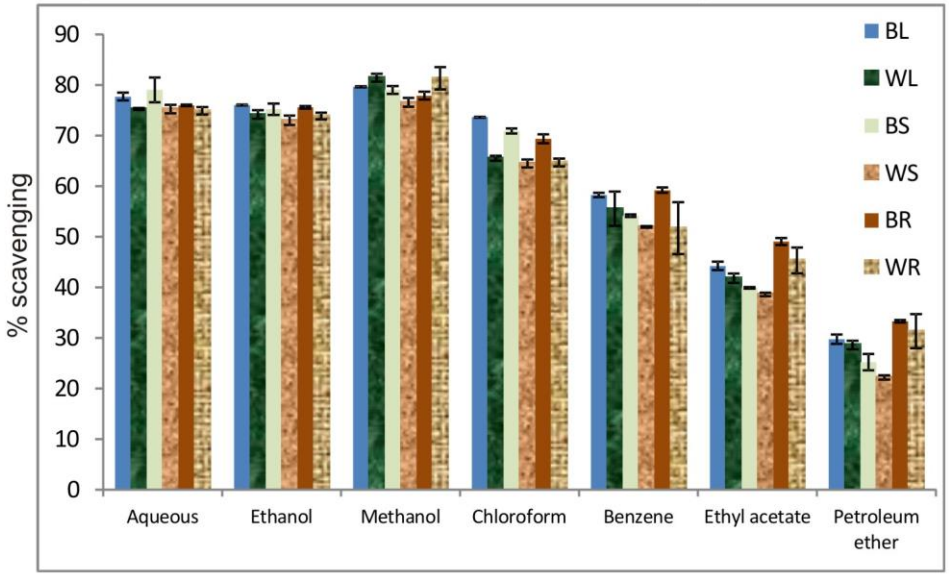

Figure 4.2

ABTS scavenging activity of different solvent extracts of leaves, seeds and roots of *Clitoria ternatea* bearing blue and white flowers

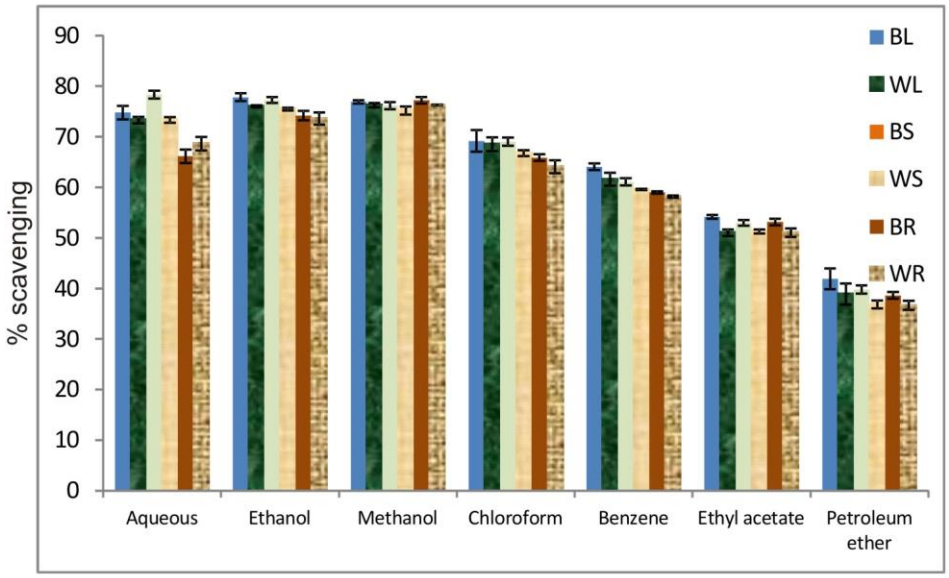

The values are mean ± SD of triplicates
BL- blue leaf extracts; WL- white leaf extracts; BS- blue seed extracts;
WS- white seed extracts; BR- blue root extracts; WR- white root extracts

Mahendran *et al*. (2015) studied the activity of isolated compounds from *Swertia corymbosa* (Grieb.) Wight *ex* C.B. Clark using *in vitro* methods like DPPH, ABTS, superoxide, nitric oxide and hydroxyl radical scavenging activities, ferric reducing antioxidant power and metal chelating ability, and found significant antioxidant activity.

Udayaprakash *et al*. (2015) studied the antioxidant and free radical scavenging potential of the methanolic leaf extract of *Cinnamomum iners* and found the maximum inhibition in ABTS assay, which proved that the plant can be potentially used as an antioxidant agent in pharmaceutical and nutraceutical industries. Kolodziejczyk-Czepas *et al*. (2015) measured the DPPH radical dot plot and ABTS radical dot plot radical scavenging activity and indicated that the *Matricaria chamomilla* L. had considerable anti-free radical action.

Ilaiyaraja *et al*. (2015) optimised the extraction conditions for the maximum recovery of polyphenols with high antioxidant activity in *Feronia limonia* fruit and showed that the concentration of ethanol and temperature affected ABTS radical scavenging activities significantly. Jøraholmen *et al*. (2015) prepared and optimized chitosan-coated liposomes with resveratrol and confirmed it to be as potent as standard antioxidants by *in vitro* anti-oxidative activities using DPPH and ABTS radicals scavenging assays.

In the present study, among the different solvent extracts analyzed, the methanolic extracts of the leaves of the both the varieties of *Clitoria ternatea* bearing blue and white flowers exhibited better oxidant-scavenging activity than the other plant parts and other solvent extracts studied. Our results are in agreement with the above-cited studies.

4.1.3 Hydroxyl radical scavenging effects:

The effect of leaf, seed and root extracts on oxidant induced damage to deoxyribose *in vitro* was quantified as the amount of thiobarbituric acid reactive substances (TBARS) formed. As hydroxyl is the most damaging free radical that can have devastating effects within the body compared to other free radicals, investigation of natural antioxidants and their capacity to scavenge hydroxyl radicals have always attracted attention (Zhuo *et al*., 2012a).

The effect of leaf extracts on hydrogen peroxide induced damage to deoxyribose was qualified as the amount of TBARS formed and the results are represented in Figure 4.3. There was a steep increase in TBARS formation when deoxyribose was exposed to hydrogen peroxide, which was effectively inhibited by all the extracts tested (leaf, seed and root extracts in different solvents). The leaf extracts showed better scavenging effect than the other two parts tested in both the varieties.

The antioxidant activity of the bioactive molecules from fruits of four varieties of *Prunus persica* at different stages of ripening (green, small orange, red) were studied by various assays including TBARS assay (Belhadj *et al*. 2016). Lima *et al*. (2015) evaluated the influences of variables of preparation on total flavonoids content from extractive solution of *Lippia sidoides* Cham., Verbenaceae and reported that the extracts exhibited a significant dose-dependent antioxidant effect as evaluated by TRAP/TAR assays.

Rakholiya *et al*. (2013) studied the antioxidant activity of mango (*Mangifera indica* L.) ripe peel by OH radical scavenging activity and found that the acetone extract showed the best antioxidant activity. Ojiako *et al*. (2015) investigated the capacity of single and combinatorial herbal formulations of *Acanthus montanus, Emilia coccinea, Hibiscus rosasinensis* and *Asystasia gangetica* using *in vitro* assays like hydroxyl radical scavenging and found that the single herbal formulations exhibited higher radical

scavenging capacities than those of the combinatorial herbal formulations. Muthu and Durairaj (2015) have reported that the 50% ethanolic extract of *Annona muricata* leaves exhibited effective radical scavenging potentials against superoxide, nitric oxide, hydroxyl and hydrogen peroxide.

El-Shora *et al*. (2015) assessed the influence of gamma radiation on the antioxidant capability of methanol extract of fenugreek (*Trigonella foenum* graecum) and reported that the free radical scavenging activity increased gradually with increasing irradiation dose up to 800 Gy. using by DPPH, superoxide radical, hydroxyl radical, ABTS, hydrogen peroxide scavenging activity, inhibition of lipid peroxidation, chelating power and FRAP assays. Vasundhara and Devi (2015) have reported a dose-dependent free radical scavenging activity of petroleum ether, chloroform, ethanol and aqueous extracts of *Boerhavia diffusa* leaves by *in vitro* methods like DPPH, ABTS, nitric oxide, hydroxyl, hydrogen peroxide and superoxide radical scavenging activity.

In vitro antioxidant activities of *Terminalia arjuna* bark were carried out by spectrophotometric methods to assess the free radical scavenging activities, such as DPPH, hydroxyl, ABTS, nitric oxide, metal chelation, FRAP and reducing power and found that the ethyl acetate fraction exhibited the maximum scavenging activity (Kumar *et al*. 2013). Khatri *et al*. (2013) investigated the *in vitro* antioxidant activities of *Indigofera cordifolia* seed extracts and reported that the methanolic extract is a more potent scavenger of hydroxyl radicals than aqueous extract and mannitol.

In our study, among the different solvent extracts analysed, the methanolic extracts of the leaves of both the varieties recorded higher oxidant-scavenging activity than the other plant parts studied, which is in agreement with the above reports.

Figure 4.3

Hydroxyl radical scavenging activity of different solvent extracts of leaves, seeds and roots of *Clitoria ternatea* bearing blue and white flowers

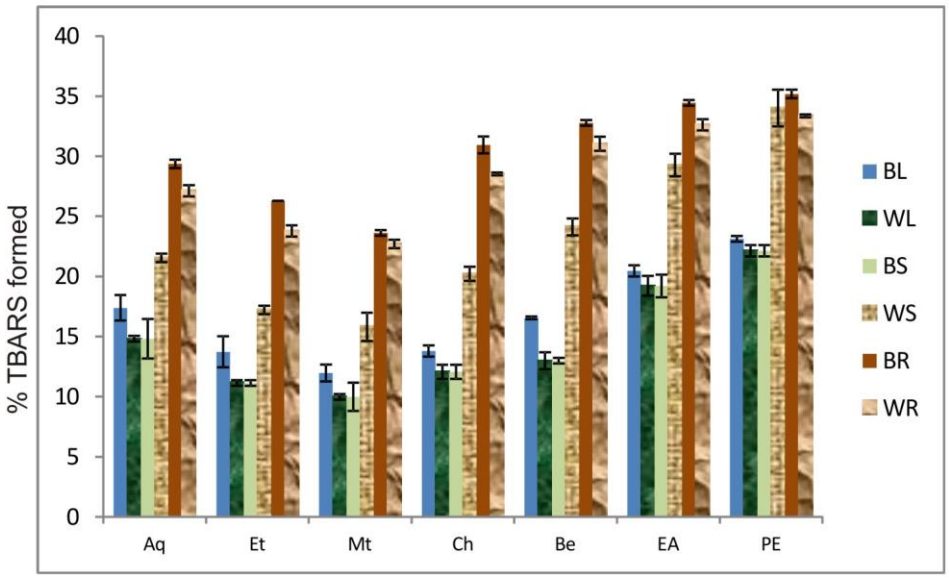

Figure 4.4

Hydrogen peroxide scavenging activity of different solvent extracts of leaves, seeds and roots of *Clitoria ternatea* bearing blue and white flowers

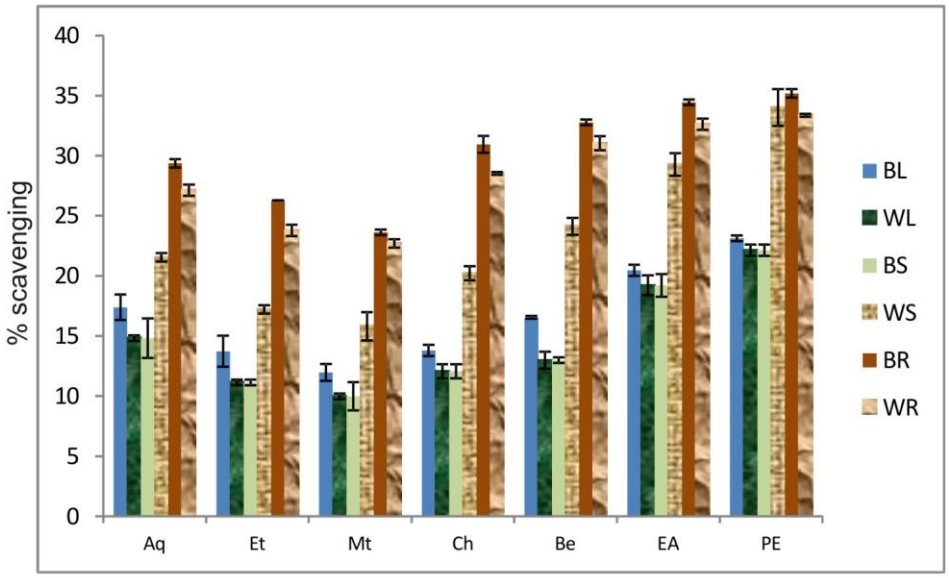

The values are mean ± SD of triplicates
BL- blue leaf extracts; WL- white leaf extracts; BS- blue seed extracts;
WS- white seed extracts; BR- blue root extracts; WR- white root extracts

4.1.4 Hydrogen peroxide scavenging effects:

The ability of the leaf, seed and root extracts to scavenge H_2O_2 was assessed. Aqueous, ethanol and methanol extracts of leaf, seed and root extracts of *Clitoria ternatea* bearing blue and white flowers scavenged hydrogen peroxide effectively compared to the other solvent extracts tested (Figure 4.4).

Al-Amiery *et al.* (2015) synthesized coumarins 1-8 using chemical and microwave-assisted methods and screened for *in vitro* scavenging activity using hydrogen peroxide and showed high scavenging activity. Dandekar *et al*. (2015) determined the free radical scavenging activity of *Epiphyllum oxypetalum* by *in vitro* methods utilizing DPPH radical scavenging assay and hydrogen peroxide scavenging assay and found that higher antioxidant activity was exhibited by the alcohol extract than the aqueous extract.

Jinu *et al*. (2015) investigated the antioxidant potential of cholestanol glucoside, a steroidal glycoside produced by *Lasiodiplodia theobromae*, an endophytic fungus isolated from *Saraca asoca*, using *in vitro* assays and found that the compound could effectively scavenge hydrogen peroxide and hydroxyl radicals. Palchoudhuri *et al*. (2016) evaluated the active phyto-constituents and *in vitro* antioxidant as well as free radical scavenging activity of aqueous root extract of *Withania somnifera* and elucidated that the root extract of *W. somnifera* possessed concentration dependent superoxide, nitric oxide and hydrogen peroxide scavenging activities.

Antioxidants act as radical scavengers, inhibit lipid peroxidation and other free radical-mediated processes, and therefore, protect the human body from several diseases attributed to the reactions of radicals. Various antioxidants have been shown to scavenge free radicals and have been explored to find therapeutic drugs for free radical pathologies (Zingare *et al*., 2013).

Comparative evaluation of *in vitro* antioxidant activity of the roots of blue and white flowered varieties of *Clitoria ternatea* showed that the methanol extracts of blue and white flowered varieties showed a very powerful antioxidant activity in DPPH radical-scavenging assay, significant reductive ability as well as hydroxyl radical scavenging activity, which was higher in the white flowered variety than the blue flowered variety (Patil and Patil, 2011). The antioxidant property of stem extracts of *Clitoria ternatea* was evaluated by DPPH free radical scavenging capacity, hydroxyl radicals scavenging capacity, superoxide radical scavenging capacity and antioxidant activity using β - carotene linoleate model system, wherein the methanolic extract showed higher free radical scavenging capacity as compared to the acetone extract (Jain *et al*., 2010).

In the present study, the extracts of leaves, seeds and roots of *Clitoria ternatea* showed good antioxidant activity. In order to test whether this potential is reflected in the bioactivity, they were assessed for the antibacterial activity using turbidity method.

4.2 ASSESSMENT OF ANTIBACTERIAL ACTIVITY:

Several pathogenic microorganisms are gaining resistance to the existing antibiotics. This has increased the interest of researchers all over the world in studying the different extracts of traditional medicinal plants as potential sources of new antimicrobial agents and search for new antimicrobial agents (Hossain *et al*., 2012).

4.2.1 Assessment of antibacterial activity by turbidity method:

The antibacterial activity of the different solvent extracts of the leaves, seeds and roots were determined by turbidity method against clinical isolates of *Escherichia coli* and *Staphylococcus aureus*. The results obtained are presented in Figures 4.5 and 4.6 respectively. It is clear from the results that methanolic leaf extracts inhibited the microbial growth to a higher extent than the other solvent extracts tested, as well as the other plant parts tested. The

inhibition of methanolic leaf extract of white variety was comparable with that of 30µg of ampicillin against both the organisms tested.

Krishnavignesh *et al*. (2013) studied *in vitro* antimicrobial activity of *Parthenium hysterophorus* L. against pathogenic microorganisms and found that the methanolic leaf extracts inhibited the growth of *Candida albicans* and *Candida glabrata* and exhibited significant activity against the human pathogens namely *E. coli, Pseudomonas* sp*., Klebsiella* sp*., Citrobacter* sp., *Streptococcus* sp., and *Enterobacter* sp. This investigation proved that the methanol extract of *Parthenium hysterophorus* L. leaves possess promising antibacterial potential against both the Gram positive and Gram negative bacteria.

As *Pyrrosia petiolosa* is commonly used as a traditional Chinese medicine for treatment of acute pyelonephritis, chronic bronchitis and bronchial asthma. Cheng *et al*. (2014) studied the antibacterial activity of the ethanol extract in comparison with the fractions obtained with solvents of different polarities and found different extracts to elicit different responses in the organisms studied. Bezzerri *et al*. (2014) studied the natural peptides with antimicrobial properties and found the peptide TB_KKG6A exhibited antimicrobial activity at low concentrations. Belhadj *et al*. (2016) studied the antibacterial activity of *Prunus persica* varieties and found that the extracts were more sensitive against *Staphylococcus aureus* and *Listeria monocytogenes*.

Govindappa *et al*. (2011) have reported the antimicrobial and antioxidant activity of ethanol extracts of *Wedelia trilobata* (L.) Hitchc. leaf, stem and flower. Rakholiya *et al*. (2013) studied the antimicrobial property of *Mangifera indica* L. ripe peel against twenty five selective microorganisms by agar well diffusion method and found that the acetone extract elicited the best antimicrobial activity.

Figure 4.5

Antibacterial activity of different solvent extracts of *Clitoria ternatea* leaf, seed and root bearing blue and white flowers against *E. coli*

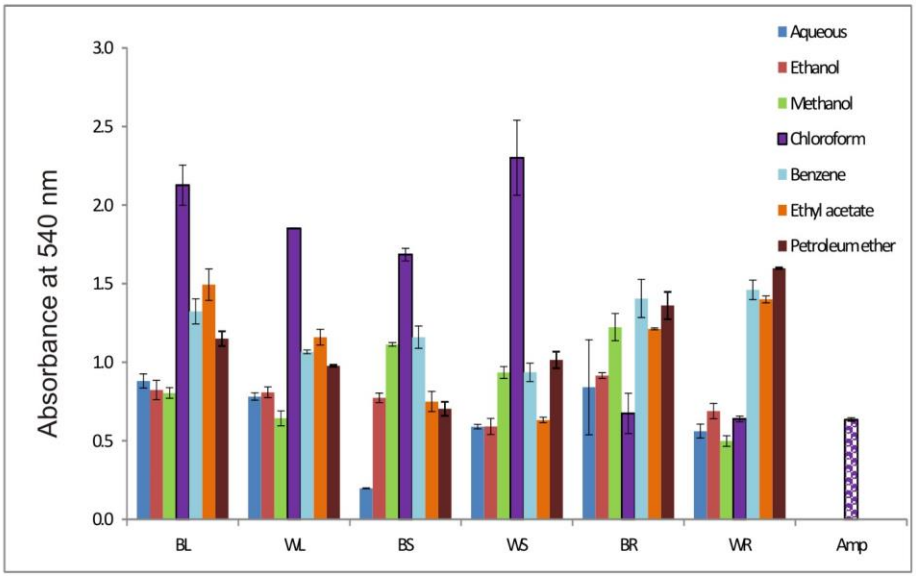

Figure 4.6

Antibacterial activity of different solvent extracts of *Clitoria ternatea* leaf, seed and root bearing blue and white flowers against *S. aureus*

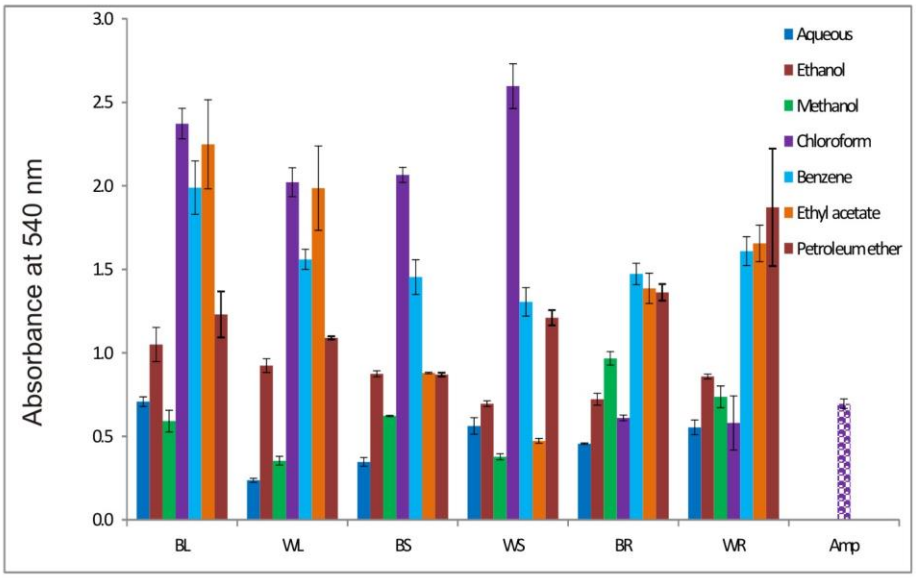

The values are mean ± SD of triplicates
BL- blue leaf extracts; WL- white leaf extracts; BS- blue seed extracts;
WS- white seed extracts; BR- blue root extracts; WR- white root extracts

Thus, the first phase of the present study clearly showed that the leaves of both the varieties of *C. ternatea* possess better antioxidant and antibacterial effects than the other plant parts tested. It was also found that the methanolic extract was more effective than the other solvent extracts. Therefore, only the methanolic extract of the leaves of both the varieties of *Clitoria ternatea* were taken for analysis in the further phases of the study, wherein the silver and gold nanobioconjugates were prepared from the extracts and analyzed for their therapeutic bioactivity.

PHASE II

4.3 SYNTHESIS OF NANOBIOCONJUGATES:

Silver and gold nanobioconjugates have been synthesized using different heating sources and different time period of exposure. In the present study, three different sources namely bright sunlight, water bath and microwave oven were selected with different time periods of exposure. The results are shown in Plates 4.1 and 4.2. Colour change of the solutions to yellowish brown and violet was observed indicating the formation of silver and gold nanobioconjugates respectively. From the results, it was clear that the direct sunlight exposure for 20 minutes gave maximum yield for both silver and gold nanobioconjugates among the different methods experimented with varying time periods of exposure. Among the two methods, a deeper colour change was observed with the gold nanobioconjugate synthesis than the silver nanobioconjugate synthesis. This observation showed that the synthesis of gold nanobioconjugates occurred more rapidly than silver nanobioconjugates.

Schliebe (2013) also reported a photochemical approach for the straight forward synthesis of Ag and Au NPs using a single source precursor under very mild conditions. Restrepo *et al*. (2012) used microwave-assisted oxidation and immobilized AuNPs on a gel-supported ionic liquid. Yasmin *et al*. (2014) synthesized AuNPs from a medicinal plant, *H. rosasinensis*, rapidly using microwave heating.

Plate 4.1

Synthesis of silver nanobioconjugates from *Clitoria ternatea* leaf extracts using different methods

Sunlight - Blue

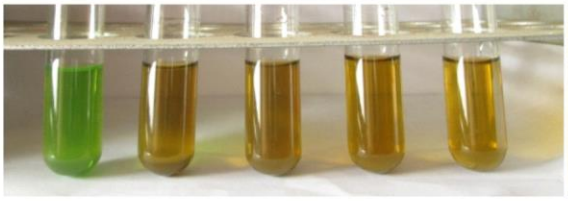

0m 5m 10m 15m 20m

Sunlight - White

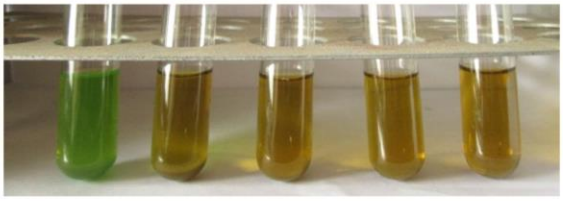

0m 5m 10m 15m 20m

Water bath - Blue

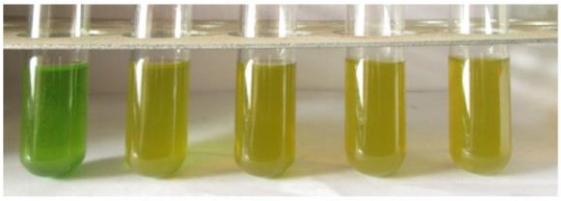

0m 5m 10m 15m 20m

Water bath - White

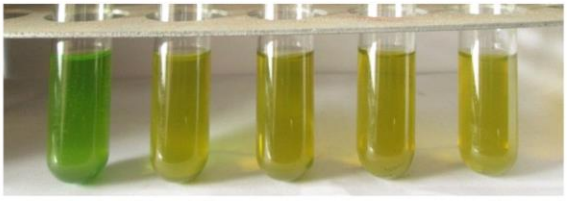

0m 5m 10m 15m 20m

Microwave - Blue

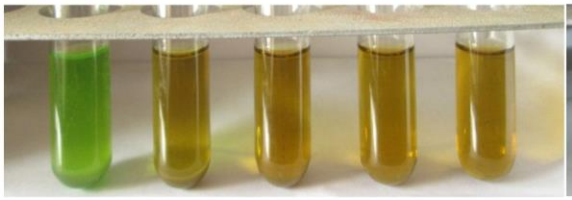

0s 10s 20s 30s 40s

Microwave - White

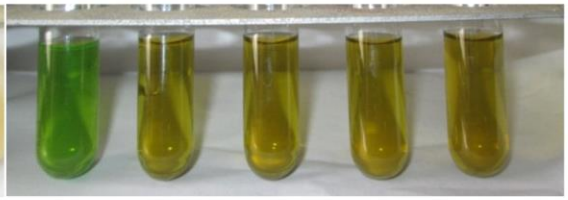

0s 10s 20s 30s 40s

Plate 4.2

Synthesis of gold nanobioconjugates from *Clitoria ternatea* leaf extracts using different methods

Sunlight - Blue

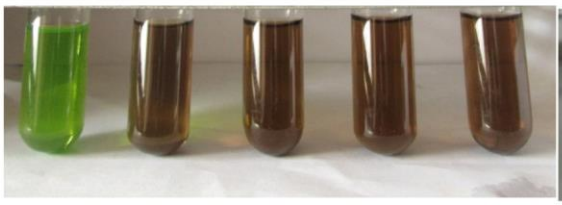

0m 5m 10m 15m 20m

Sunlight - White

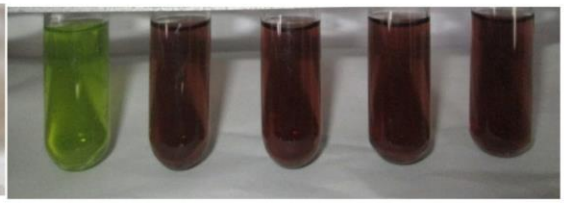

0m 5m 10m 15m 20m

Water bath - Blue

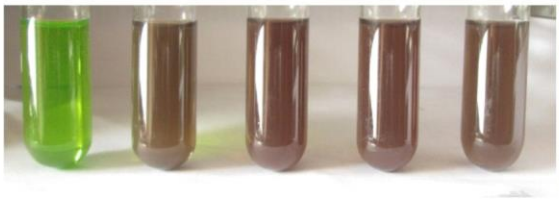

0m 5m 10m 15m 20m

Water bath - White

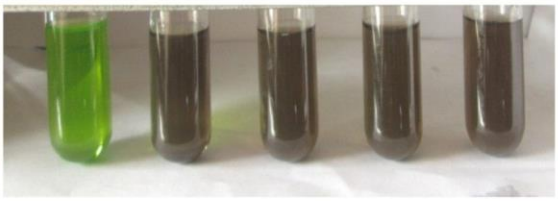

0m 5m 10m 15m 20m

Microwave - Blue

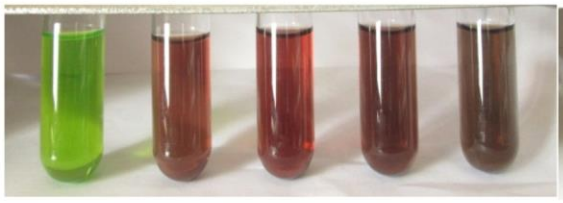

0s 10s 20s 30s 40s

Microwave - White

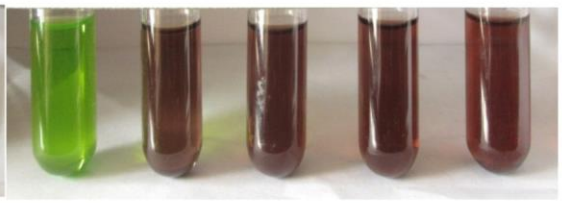

0s 10s 20s 30s 40s

Plants and plant extracts can be effectively used in the synthesis of gold and AgNPs as a greener route. Shape and size control of NPs is easily understood with the use of plants. The NPs extracted from plants are used in many AuNP formation by oat and wheat applications for benefit of humans (Vadlapudi and Kaladhar, 2014). Isaac *et al*. (2013) reported a one-step green synthesis of gold and silver nanoparticles using fruit extract of *Averrhoa bilimbi* L. using the colour change of solutions to yellow and violet, indicating the formation of silver and gold NPs respectively. El-Naggara *et al*. (2016) also used eco-friendly microwave-assisted green and rapid synthesis of well-stabilized gold and core-shell silver-gold nanoparticles.

4.3.1 Separation and yield of nanobioconjugatess:

The nanobioconjugates were separated by centrifugation, washed, dried and weighed to calculate the yield. The gold nanobioconjugates gave maximum yield compared to silver nanobioconjugates and the white variety gave maximum yield compared with methanolic leaf extracts of *Clitoria ternatea* bearing blue flowers (Table 4.1).

Table 4.1: Per cent yield of silver and gold nanobioconjugates by different methods of synthesis

Methods	Duration	% yield (mg)			
		AgB	AgW	AuB	AuW
Sunlight	5 minutes	12.4	12.6	14.2	14.4
	10 minutes	17.5	17.6	18.5	18.7
	15 minutes	21.3	21.5	23.9	24.1
	20 minutes	25.5	25.3	26.1	26.3
Water bath	5 minutes	7.2	7.4	8.6	8.9
	10 minutes	11.2	11.5	12.3	12.5
	15 minutes	15.4	15.8	16.6	16.9
	20 minutes	20.0	20.2	21.8	21.9
Microwave	10 seconds	9.2	9.3	9.8	10.1
	20 seconds	14.2	14.2	15.1	15.4
	30 seconds	18.5	18.7	19.3	19.6
	40 seconds	22.2	22.4	24.4	24.7

The synthesis using sunlight for 20 minutes gave maximum yield when compared with other methods and duration of exposure. Therefore, this method was taken as the method of choice for further experiments in the study. The synthesized nanobioconjugates were then characterized using a spectrum of physicochemical methods.

4.4 CHARACTERIZATION OF NANOPARTICLES:

The silver and gold nanobioconjugates synthesized were characterized using UV-Visible absorption spectroscopy, TEM, SEM, EDX, XRD, Zeta potential and Poly Dispersity Index, as the characterization is necessary to find out the size, shape, stability and other specifications of NPs before screening their bioactivity or utilizing it. The results obtained are presented below.

4.4.1 UV-Visible Absorption Spectroscopy:

Nanoparticles exhibit unique, tunable optical properties on the basis of their Surface Palsmon Resonance. Nanoparticles synthesized in the present study, using different methods with varying time of exposure, were subjected to spectral analysis using UV-Visible Nanophotometer (Optizen, Korea) in a range of 220 nm to 800 nm. Silver and gold nanobioconjugates gave characteristic peaks. The results are presented in Figures 4.7 and 4.8. The results revealed that the synthesis using sunlight for 20 minutes gave maximum yield when compared with other methods (water bath and microwave) and other incubation times (5, 10, 15 minutes).

Behera and Nayak (2013) synthesized AgNPs using jamun extract and characterized using UV-Visible spectroscopy, where high band intensities and peaks were observed under visible spectrum at 422 nm. Lin *et al*. (2013) used UV-Visible absorption spectroscopy and found an increase in the growth of AuNPs as the amount of $NaBH_4$ increases while preparing it by reducing $HAuCl_4$.

Figure 4.7

Absorption spectrum of silver nanobioconjugates synthesized from *Clitoria ternatea* leaves bearing blue and white flowers

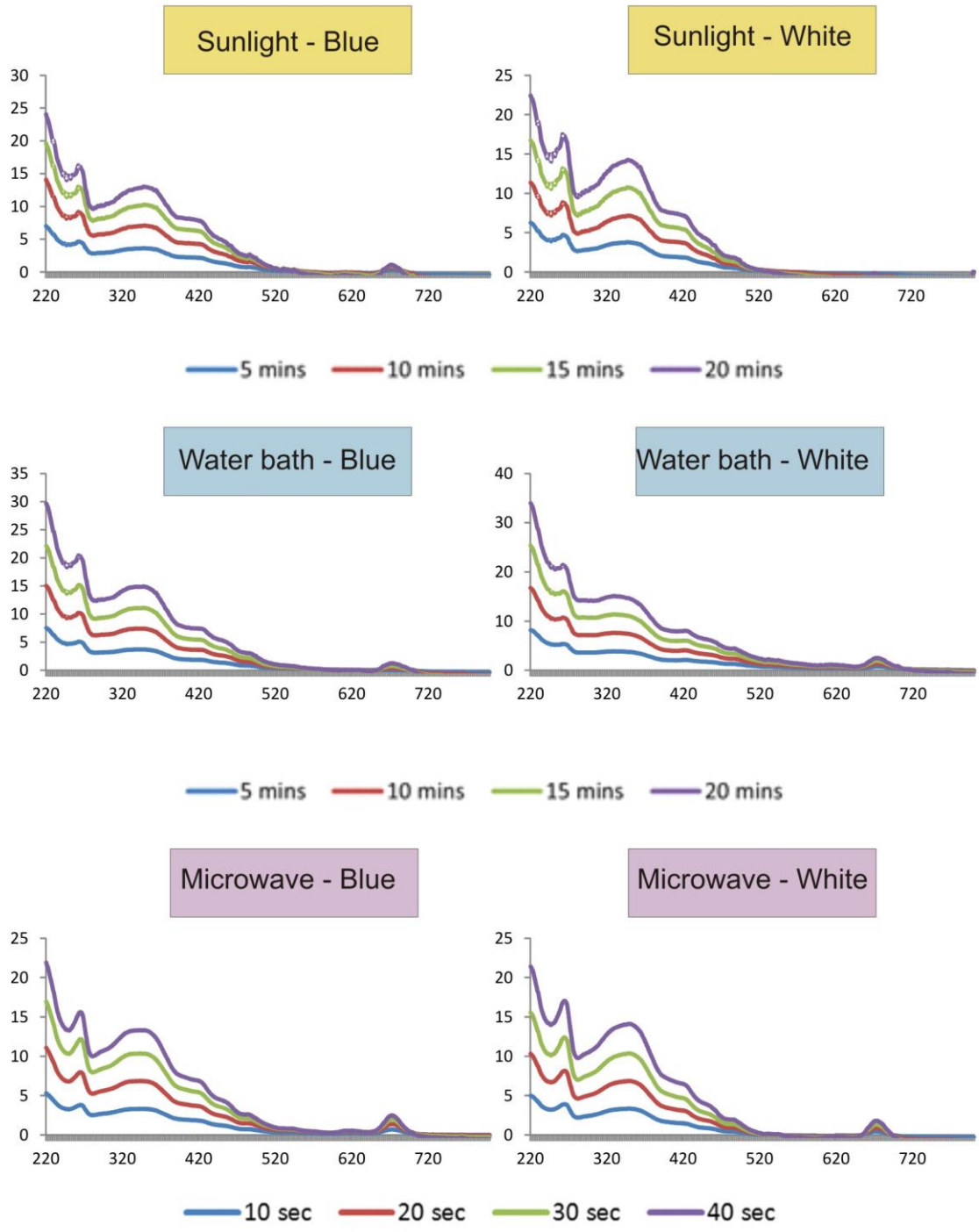

Figure 4.8

Absorption spectrum of gold nanobioconjugates synthesized from *Clitoria ternatea* leaves bearing blue and white flowers

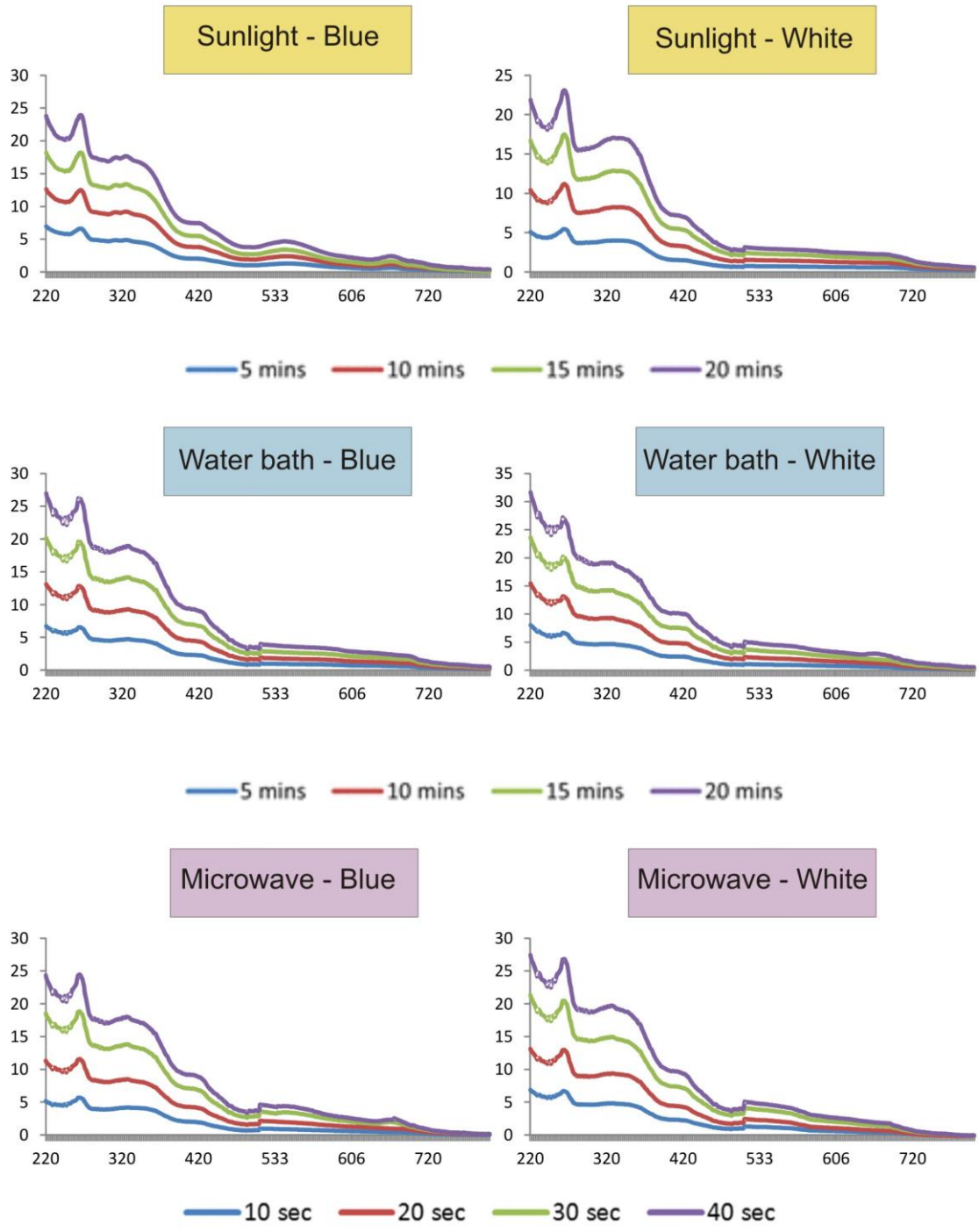

Nima and Ganesan (2015) found high SPR vibrations at 410 and 535nm respectively by UV-Visible spectroscopic analysis of silver and gold NPs synthesized from *Couroupita guianensis* flower bud. Khachatryan *et al*. (2016) prepared silver and gold nanoparticles embedded in potato starch matrix and studied the absorption using UV-Visible absorption spectroscopy.

Chitte *et al*. (2012) synthesized AgNPs by chemical reduction method from polymeric composites of polyvinyl alcohol, poly pyrrole and carboxy methyl cellulose and characterized using UV-Visible absorption spectroscopy, which showed characteristic absorption band at 420 nm confirming the formation of silver NPs. Wanninayake *et al*. (2015) also found characteristic peak at 540 nm for AuNPs in the UV-Visible spectrum. Singh *et al*. (2016) synthesized silver and gold NPs using *Sporosarcina koreensis* and characterized them by UV-Visible spectrophotometry, which displayed maximum absorbance at 424 nm and 531 nm for silver and gold nanoparticles, respectively.

Our study also showed characteristic absorption spectra for the nanobioconjugates synthesized, with a higher absorption in the sunlight-exposed leaf extract mixtures. This shows that the most effective method for the green synthesis of the nanobioconjugates using silver and gold was the exposure to bright sunlight for 20 minutes.

4.4.2 Transmission electron microscopy (TEM):

The TEM images of the silver and gold nanobioconjugates of both the varieties of *Clitoria ternatea* leaf extracts were recorded, using which the particle size and shape of the nanobioconjugates were determined. Silver nanobioconjugates synthesized using the methanolic leaf extract of *Clitoria ternatea* bearing blue flowers were found to have a particle size between 10.4 nm - 14.2 nm and silver nanobioconjugates synthesized using the methanolic leaf extract of *Clitoria ternatea* bearing white flowers were found to have

particle size between 17.6 nm - 19.4 nm. Both the silver nanobioconjugates exhibited a spherical shape (Plate 4.3).

Gold nanobioconjugates synthesized using the methanolic leaf extract of *Clitoria ternatea* bearing blue flowers were found to have a particle size between 22.2 nm - 46.2 nm and those from plants bearing white flowers were found to have a particle size between 16.4 nm - 22.3 nm (Plate 4.5b). Our results clearly show that both the silver and the gold nanobioconjugates prepared from *Clitoria ternatea* leaf extract were well within the nanoscale (<100nm). This also implies that they will have easier penetrating power into the cell (Haider and Kang, 2015).

Chitte *et al*. (2012) also used TEM image to find out the particle size and shape of silver nanoparticle and observed nanoparticles of different sizes in the range from 40 nm – 80 nm which were synthesized by chemical reduction method from polymeric composites of polyvinyl alcohol, poly pyrrole and carboxy methyl cellulose. Lin *et al*. (2013) prepared AuNPs by reducing $HAuCl_4$ with different amounts of $NaBH_4$. Using TEM images, found that the sizes of AuNPs can be tuned by adjusting the amount of $NaBH_4$ added. Behera and Nayak (2013) synthesized AgNPs through jamun extract and found irregular shapes with size varying from 30 - 100 nm by TEM analysis.

Zhou *et al*. (2012b) synthesized silver and gold nanoparticles of citrate and characterized by TEM analysis. Khachatryan *et al*. (2016) prepared silver and gold nanoparticles embedded in potato starch matrix and characterized them using TEM and reported well separated and spherical with a size of 10 to 20 nm for both silver and gold nanostructures. Singh *et al*. (2016) synthesized Ag and Au nanoparticles using *Sporosarcina koreensis* strain and observed spherical shape of NPs by field emission transmission electron microscopy.

Plate 4.3

TEM images of silver nanobioconjugates of *Clitoria ternatea* leaf extracts bearing blue (AgB) and white (AgW) flowers

a) Silver nanobioconjugates of blue variety (AgB)

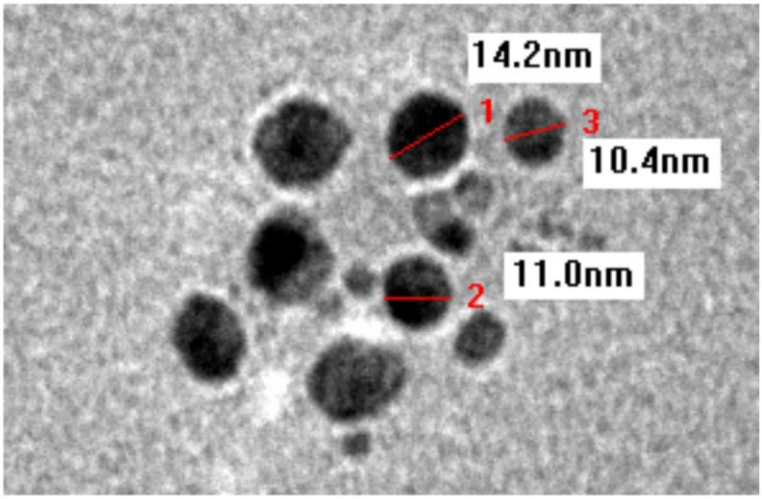

b) Silver nanobioconjugates of white variety (AgW)

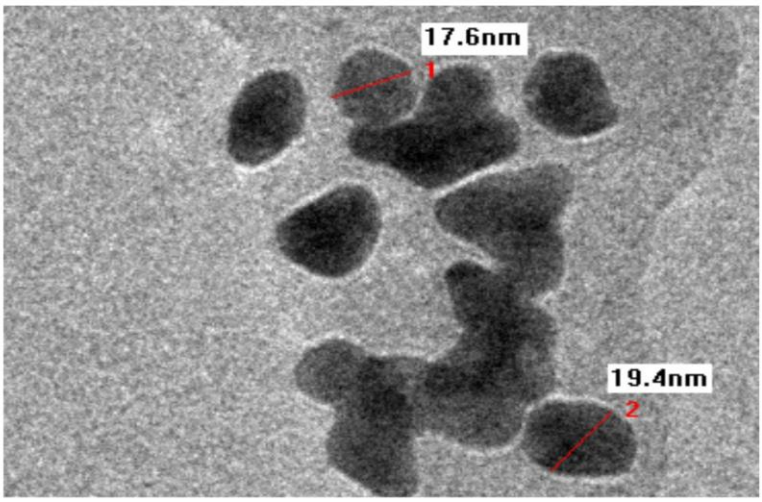

Plate 4.4

TEM images of gold nanobioconjugates of *Clitoria ternatea* leaf extracts bearing blue (AuB) and white (AuW) flowers

a) Gold nanobioconjugates of blue variety (AuB)

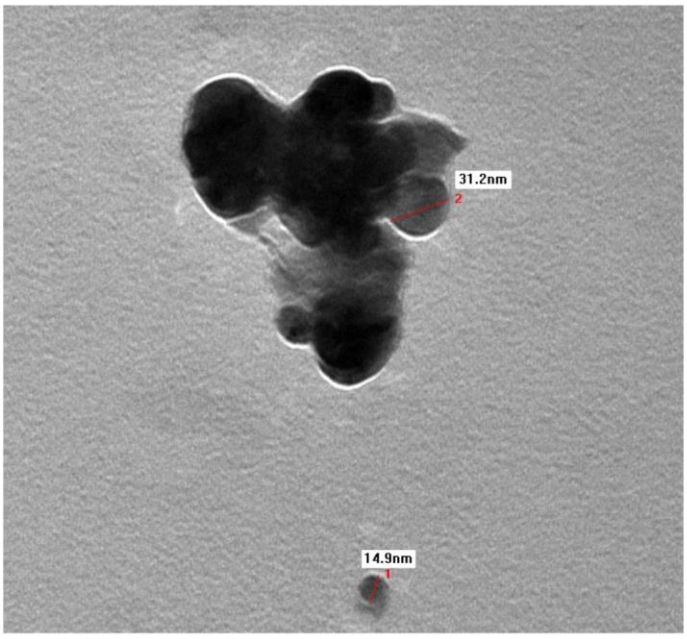

b) Gold nanobioconjugates of white variety (AuW)

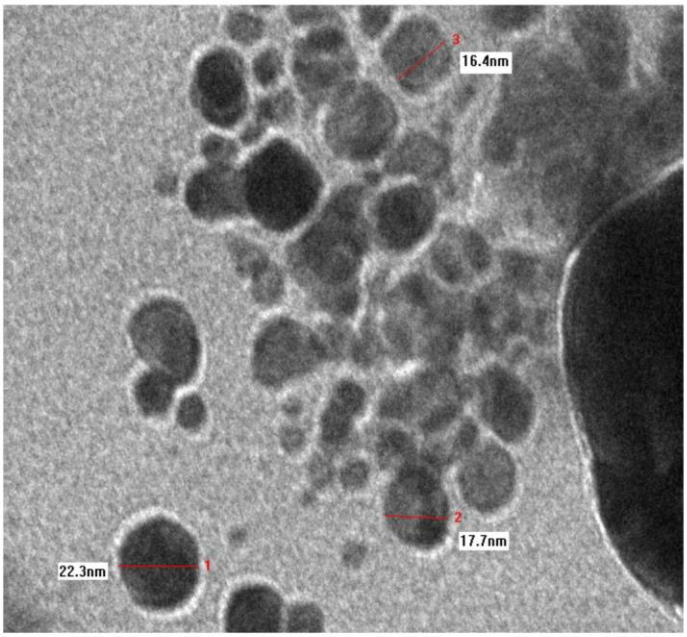

4.4.3 Field Emission Scanning electron microscopy (FESEM) with energy dispersive X-ray (EDX):

The characterization of the morphology of nanoparticles is becoming a task to be performed not only using TEM, but also more and more using modern, high-resolution scanning electron microscopes. A SEM is probably the most widespread analytical instrument available in analytical laboratories destined to characterize physical properties such as morphology, shape, size and distribution of materials at the micro and nano-scale. The performance of a modern, high-resolution SEM, in particular its spatial resolution, can reach to enable the identification and even morphology characterization of nanoparticles down and below 10 nm (Hodoroaba *et al*., 2012).

The SEM images of the silver and gold nanobioconjugates synthesized using the methanolic leaf extracts of *Clitoria ternatea* bearing blue flowers and white flowers also showed a spherical shape (Plates 4.5 and 4.6). Nadagouda *et al*. (2014) also synthesised silver and gold nanobioconjugates using antioxidants from blackberry, blueberry, pomegranate, and turmeric extracts and characterized using SEM imaging.

The EDX profile of the four nanobioconjugates was studied to find out the composition. The profiles showed typical peak patterns of silver and gold peaks, with additional peaks that corresponded to the chemical elements of organic matter like carbon and oxygen (Figures 4.9 and 4.10). These patterns clearly demonstrated that effective conjugation between silver/gold with the biomaterial, resulting in the synthesis of bioactive nanobioconjugates had occurred. The XRD patterns of nanobioconjugates confirm the presence of silver, gold and organic material and the crystalline nature of the same.

Plate 4.5

SEM images of silver nanobioconjugates of *Clitoria ternatea* leaf extracts bearing blue (AgB) and white (AgW) flowers

a) Silver nanobioconjugates of blue variety (AgB)

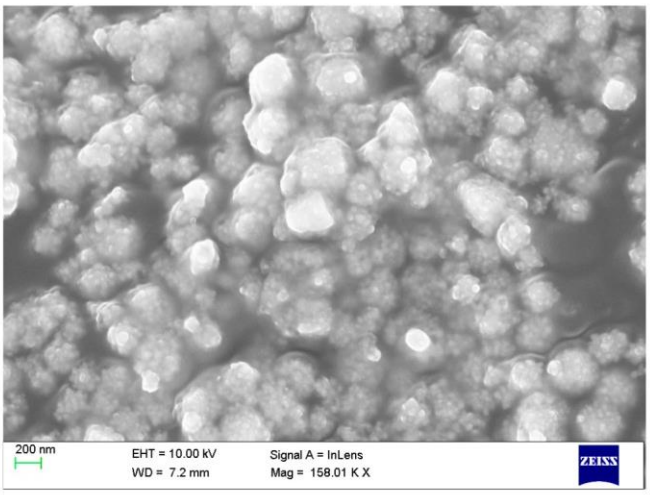

b) Silver nanobioconjugates of white variety (AgW)

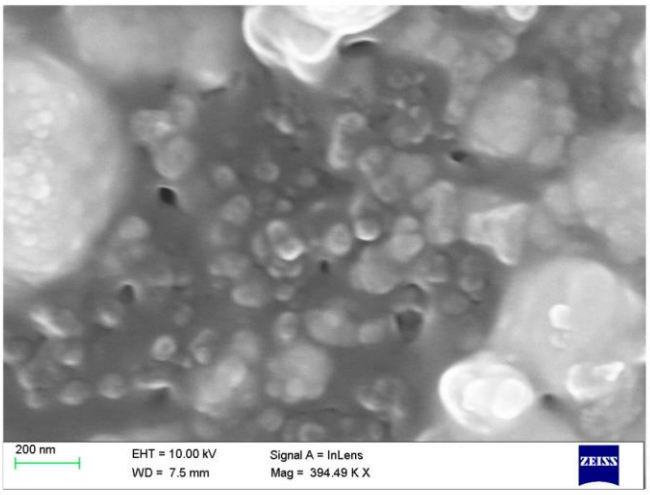

Plate 4.6

SEM images of gold nanobioconjugates of *Clitoria ternatea* leaf extracts bearing blue (AuB) and white (AuW) flowers

a) Gold nanobioconjugates of blue variety (AuB)

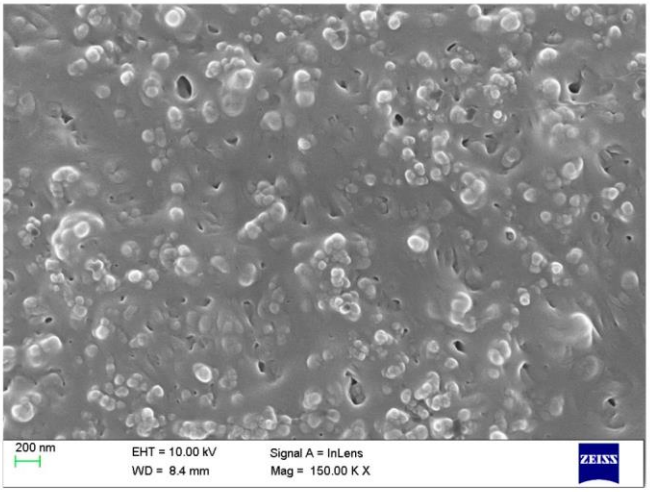

b) Gold nanobioconjugates of white variety (AuW)

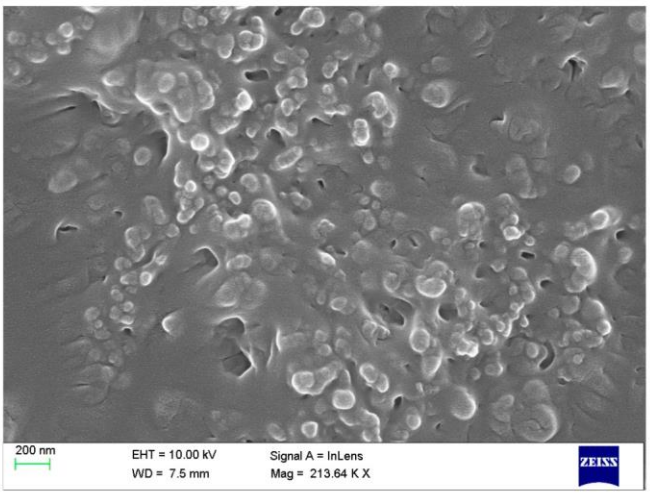

Figure 4.9

EDX spectrum of silver nanobioconjugates synthesized from *Clitoria ternatea* leaves bearing blue (AgB) and white (AgW) flowers, and their elemental composition

a) Silver nanobioconjugates of blue variety (AgB)

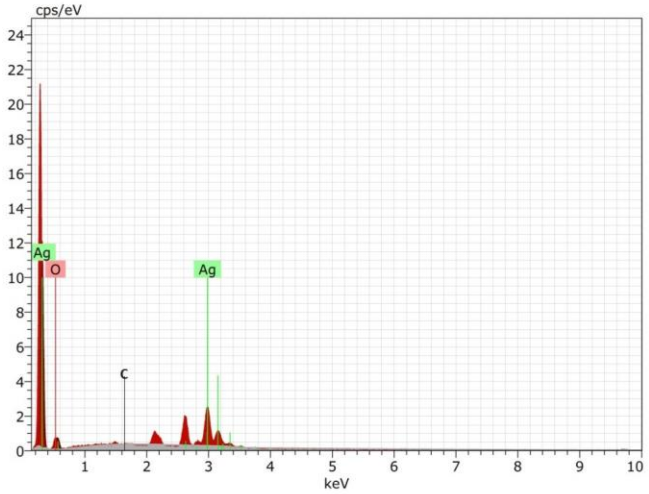

Element	wt. %	at.%
Carbon	13.51	11.23
Oxygen	11.42	47.62
Silver	75.07	41.15

b) Silver nanobioconjugates of white variety (AgW)

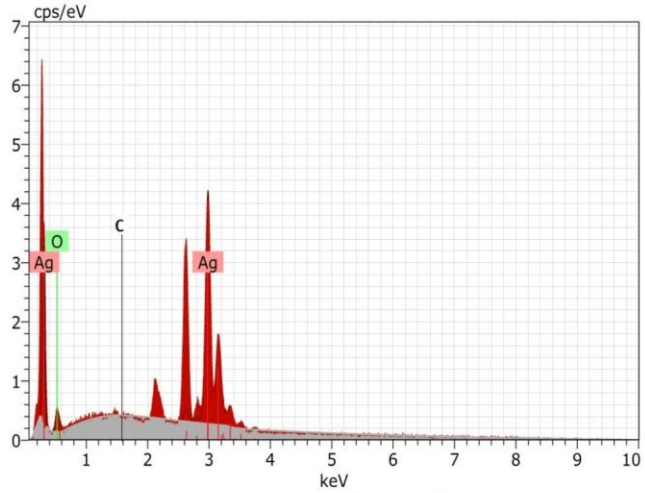

Element	wt. %	at.%
Carbon	7.21	11.41
Oxygen	3.62	21.07
Silver	89.17	67.52

Figure 4.10

EDX spectrum of gold nanobioconjugates synthesized from *Clitoria ternatea* leaves bearing blue (AuB) and white (AuW) flowers and their elemental composition

a) Gold nanobioconjugates of blue variety (AuB)

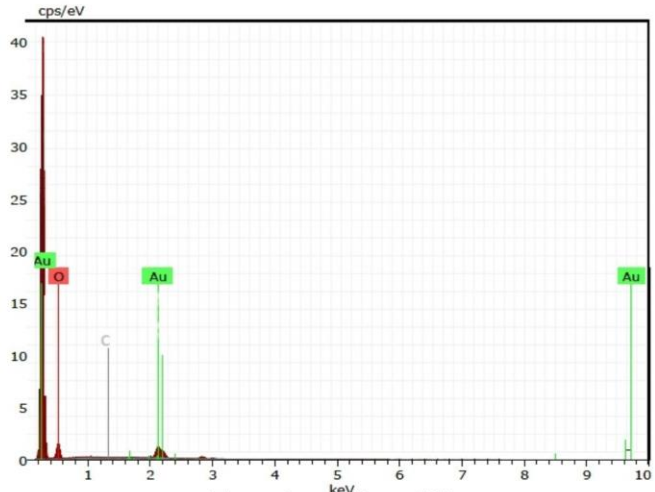

Element	wt. %	at.%
Carbon	13	61.77
Oxygen	24	24.01
Gold	63	61.77

b) Gold nanobioconjugates of white variety (AuW)

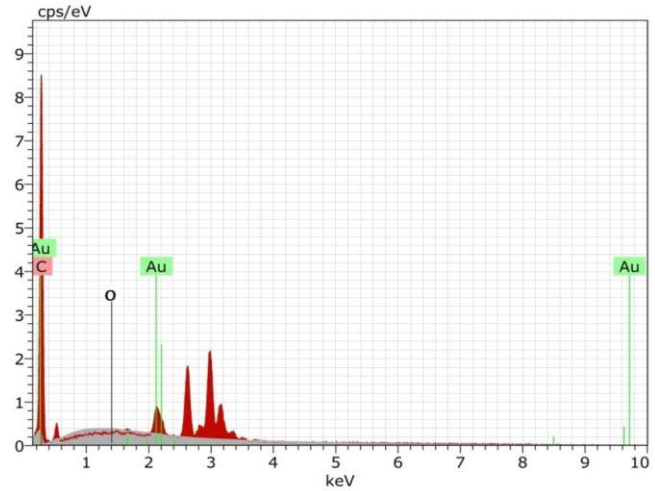

Element	wt. %	at.%
Carbon	62.41	61.41
Oxygen	8.12	16.11
Gold	29.47	22.48

Chitte *et al*. (2012) studied the SEM image of AgNPs synthesized from polymeric composites of polyvinyl alcohol, poly pyrrole and carboxy methyl cellulose by chemical reduction method. AgNPs synthesized using plants extracts of the *O. tenuiflorum*, *S. tricobatum*, *S. cumini*, *C. asiatica* and *C. sinensis* showed well dispersed nanoparticles by SEM analysis (Logeswari *et al*., 2015).

Vetrivel *et al*. (2015) observed hexagonal shaped NPs in the SEM image. Verma and Mehata (2016) obtained AgNPs using aqueous extract of Neem (*Azadirachta indica*) leaves and silver salt, which were spherical in shape and crystalline in nature, under SEM. Scibilia *et al*. (2016) studied the influence of different phage suspension buffers (i.e. the influence of different ions and medium pH) on the self-assembly of AgNPs and bacteriophage and characterized them using SEM.

The AgNPs synthesized from three endophytic fungi *Aspergillus tamarii*, *Aspergillus niger* and *Penicllium ochrochloron* isolated from an ethno-medicinal plant *Potentilla fulgens* L. were also characterized using SEM in conjunction with EDX for the elemental analysis (Devi and Joshi, 2015). Das *et al*. (2015) prepared AgNPs using *Ocimum gratissimum* leaf extract and studied their EDX. Terborg *et al*. (2015) also synthesized AuNPs and analyzed their elemental composition using EDX.

In our study also, SEM, in conjunction with EDX, was affectively used to characterize the silver and gold nanobioconjugates synthesized from the methanolic extracts of *Clitoria ternatea* leaves.

4.4.4 X-Ray Diffraction (XRD):

XRD is used to find out average particle size for a bulk sample and can identify individual crystals. The XRD spectrum of silver nanobioconjugates synthesized from blue variety was compared with the spectrum of standard silver (Figure 4.11). It showed 3 major peaks at 27.86 °2Th, 32.14 °2Th, 46.28 °2Th and 5 minor peaks. All the 3 major peaks and 5 minor peaks (except one

peak at 38.14 °2Th) matched with the peaks of standard silver and can be indexed to (111), (002), (002), (113), (222), (004) and (024).

The XRD spectrum of silver nanobioconjugates synthesized from white variety was compared with the spectrum of standard silver (Figure 4.11). It showed 3 major peaks at 27.86 °2Th, 32.14 °2Th, 46.28 °2Th and 7 minor peaks. All the 3 major peaks and 5 minor peaks (except two peaks at 38.14 °2Th and 64.6 °2Th) matched with the peaks of standard silver and can be indexed to (111), (002), (002), (113), (222), (004) and (024).

The XRD spectrum of gold nanobioconjugates synthesized from blue variety was compared with the spectrum of standard gold (Figure 4.12). It showed 2 major peaks at 26.83 °2Th, 38.16 °2Th and 6 minor peaks. One of the major peak and 5 minor peaks (except peaks at 28.24 °2Th and 32.22 °2Th) matched with the peaks of standard gold and can be indexed to (111), (002), (112), (220), (12-2), (004) and (15-1).

The XRD spectrum of gold nanobioconjugates synthesized from white variety was compared with the spectrum of standard gold (Figure 4.12). It showed 3 major peaks at 27.93 °2Th, 32.39 °2Th, 38.35 °2Th and 5 minor peaks. One of the major peaks (38.35 °2Th) and 3 minor peaks (46.32 °2Th, 54.93 °2Th and 57.57 °2Th) matched with the peaks of standard gold and can be indexed to (112), (12-2), (04-1) and (230). Thus, the XRD analysis confirmed the presence of silver and gold in the synthesized silver nanoparticles and gold nanobioconjugates respectively.

Banala *et al*. (2015) also used X-ray diffraction, EDX and FTIR analysis to characterize of *Carica papaya* leaf extract coated silver nanoparticles and found diffraction peaks at 38.2°2Th, 44.4°2Th, 64.6°2Th, 77.5°2Th, and can be indexed to (111), (200), (220), (311), and (222) planes of pure silver ions by XRD data indicating the biosynthesis of silver nanoparticles. Atta *et al*. (2013) found the formation of functionalization compound between sodium gold salt and some amino acids, which depended on the pH of the amino acid solution and associated zwitterionic forms.

Figure 4.11

XRD spectrum of silver nanobioconjugates synthesized from *Clitoria ternatea* leaves bearing blue (AgB) and white (AgW) flowers in comparison with that of silver (Ag)

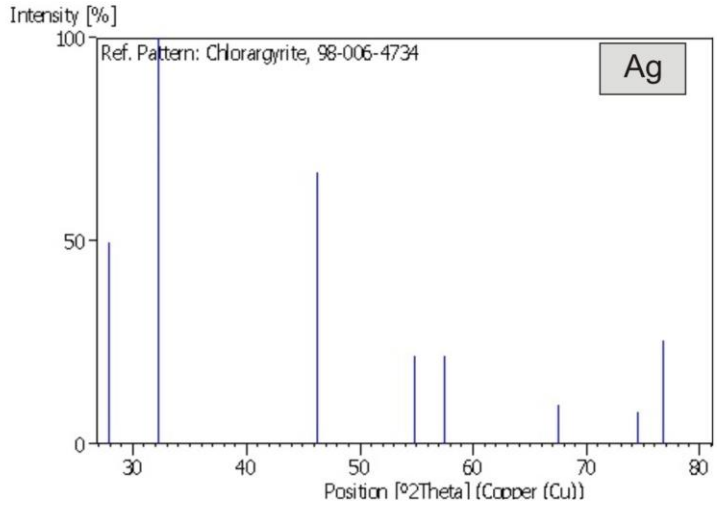

hkl	d [A]	2Theta[deg]	I [%]
111	3.20372	27.825	49.6
002	2.77450	32.238	100.0
022	1.96187	46.237	66.9
113	1.67309	54.827	21.7
222	1.60186	57.486	21.7
004	1.38725	67.459	9.5
133	1.27303	74.471	7.9
024	1.24079	76.751	25.4
224	1.13268	85.698	18.9

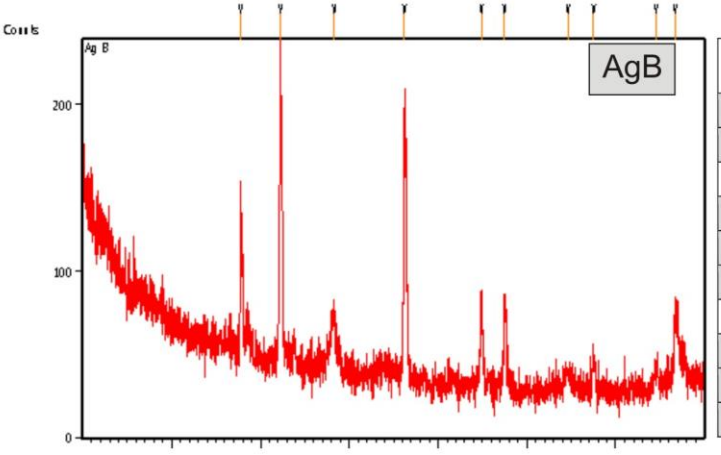

Pos. [°2Th.]	Height [cts]	FWHMLeft [°2Th.]	d-spacing [Å]	Rel. Int. [%]
27.7699	82.07	0.1338	3.21259	42.47
32.2403	193.21	0.2007	2.77663	100.00
38.3355	31.79	0.4684	2.34802	16.45
46.2185	140.55	0.2342	1.96424	72.74
54.8796	47.84	0.2676	1.67298	24.76
57.4335	51.08	0.2342	1.60452	26.44
64.6050	10.62	0.8029	1.44265	5.50
67.5053	21.04	0.4015	1.38755	10.89
74.5500	11.41	08029	1.27293	5.90
76.7025	41.14	0.4684	1.24248	21.29

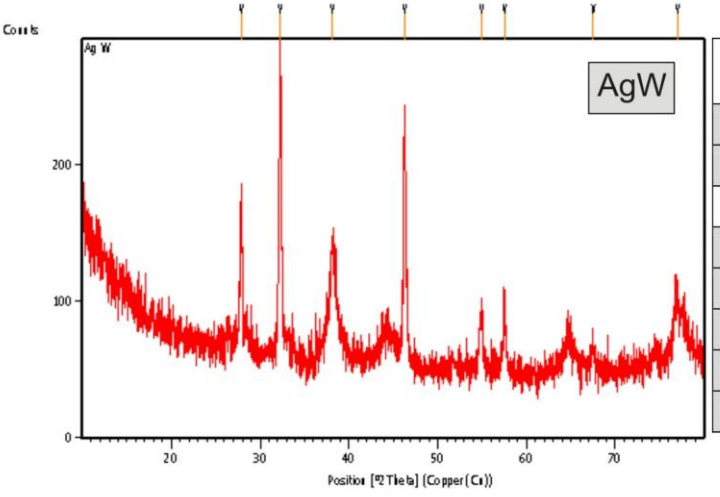

Pos. [°2Th.]	Height [cts]	FWHMLeft [°2Th.]	d-spacing [Å]	Rel. Int. [%]
27.8616	111.23	0.1673	3.20224	51.04
32.2494	217.95	0.2676	2.77586	100.00
38.1355	79.99	0.2676	2.35987	36.70
46.2840	161.49	0.2342	1.96161	74.10
54.9392	43.95	0.3346	1.67131	20.16
57.4965	52.37	0.2007	1.60291	24.03
67.5041	16.18	0.4015	1.38758	7.43
76.9976	42.32	0.4684	1.23846	19.42

Figure 4.12

XDR spectrum of gold nanobioconjugates synthesized from *Clitoria ternatea* leaves bearing blue (AuB) and white (AuW) flowers in comparison with that of gold (Au)

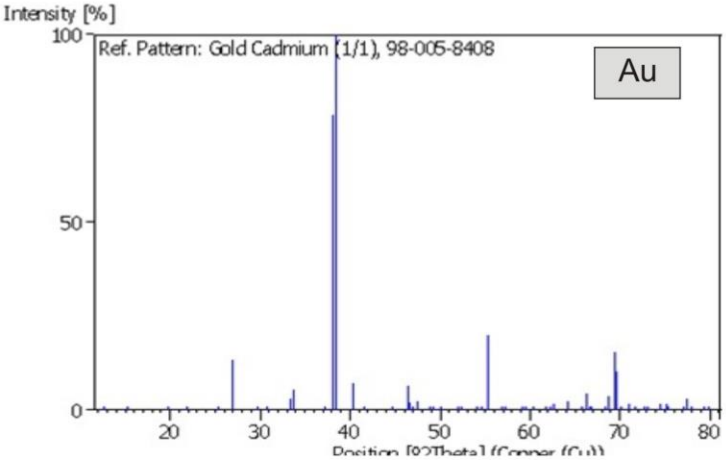

hkl	d [A]	2Theta [deg]	I [%]
11-1	3.32139	26.820	13.5
112	2.35754	38.142	78.6
220	2.02625	44.687	0.0
12-2	1.95699	46.359	6.6
023	1.69272	54.138	0.1
04-1	1.67952	54.599	0.2
230	1.61030	57.156	0.9
004	1.44925	64.216	2.4
15-1	1.23188	77.409	0.1
33-2	1.22439	77.972	0.0

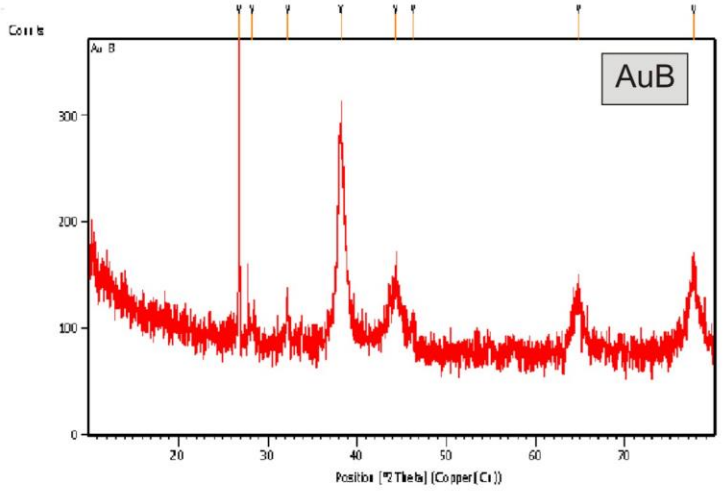

Pos.[°2Th.]	Height [cts]	FWHM Left [°2Th.]	d-spacing [Å]	Rel. Int. [%]
26.8296	150.80	0.1004	3.32302	81.83
28.2424	15.21	0.8029	3.15992	8.25
32.2199	41.51	0.2676	2.77834	22.53
38.1613	184.28	0.6022	2.35834	100
44.3144	49.49	0.5353	2.04412	26.85
46.2686	17.92	0.4015	1.96223	9.72
64.8051	48.54	0.6691	1.43868	26.34
77.6299	59.80	0.6691	1.22994	32.45

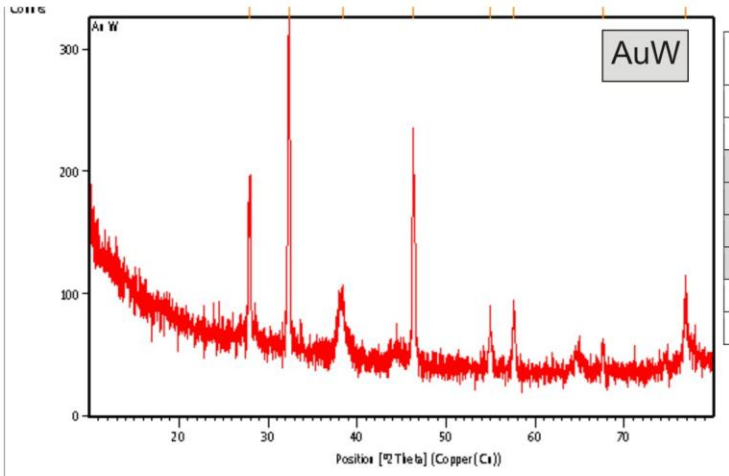

Pos.[°2Th.]	Height [cts]	FWHM Left [°2Th.]	d-spacing [Å]	Rel. Int. [%]
27.9349	115.25	0.1673	3.19399	44.17
32.3928	260.92	0.2007	2.76390	100
38.3479	47.72	0.6022	2.34729	18.29
46.3215	180.38	0.1673	1.96011	69.13
54.9340	46.88	0.2676	1.67145	17.97
57.5745	47.96	0.2342	1.60092	18.38
67.5972	21.47	0.2676	1.38589	8.23
76.8099	57.88	0.3346	1.24101	22.18

Ibrahim (2015) confirmed the crystalline nature of AgNPs by analyzing the XRD pattern and found four distinct diffraction peaks at 2θ values of 38.15º, 44.30º, 64.53º and 76.96º, which could indexed to the (111), (200), (220) and (311) reflection planes of face centered cubic structure of silver. Nima and Ganesan (2015) studied the crystalline nature of metallic silver and gold nanoparticles by XRD and reported that the spectra of representative silver and gold NPs corresponded to the 2θ = 38º (111), 46º (200), in a lattice plane and gold which are corresponding to the 2θ = 38º (111), 44º (200), 64º (220) and 77º (311) of many Bragg's reflections.

Our results with XRD clearly showed the successful conjugation of silver / gold with the components of the methanolic leaf extracts of *Clitoria ternatea*.

4.4.5 Fourier Transform Infrared Spectroscopy (FTIR) Analysis:

FTIR is one of the most widely used tools for the detection of functional groups in pure compounds and mixtures and for compound comparison. FTIR analysis was carried out for the extracts and their nanobioconjugates and compared to identify the functional groups involved in the synthesis of nanoparticles. The FTIR spectra in the mid-infrared region (4000 cm^{-1} to 800 cm^{-1}) was recorded for nanoparticles as well as the plant extracts for the functional groups identification. Characteristic functional groups contributing to the formation of absorption bands at specific wavenumbers are indicated in Figures 4.13 and 4.14.

The unbonded or “free” hydroxyl group of phenols absorbs strongly in the 3640 cm^{-1} to 3610 cm^{-1} region. Intermolecular hydrogen bond appears at lower frequencies, 3500 cm^{-1} to 3200 cm^{-1}. The leaf extracts of plant bearing blue flower had two peaks at 3356 cm^{-1} and 3302 cm^{-1} and the leaf extracts of plants bearing white flower had a peak at 3317 cm^{-1} indicating that the plant extracts have intermolecular phenolic (OH) groups in them.

The region 3300 cm^{-1} to 3000 cm^{-1} is characteristic for C-H stretching vibrations of C ≡ C, C = C and Ar-H. No bands were identified in this region for both the leaf extracts, AgB and AuW. But there were minor peaks in AgW (three peaks) and AuB (two peaks). The region from 3000 cm^{-1} to 2700 cm^{-1} is dominated by the C-H stretching vibrations of $-CH_3$, $>CH_2$, CH and CHO functional groups respectively. There were four, three and two minor peaks in gold nanobioconjugates, silver nanobioconjugates and their unconjugated leaf extract respectively.

The region between 1800 cm^{-1} and 1500 cm^{-1} show characteristic bands for proteins, wherein 1700 cm^{-1} to 1600 cm^{-1} is specific for amide-I bands, which is mainly due to C = O stretching vibrations of peptide bond. The bands in the amide I region provide insight into the protein secondary structure. On the other hand, the region from 1600 cm^{-1} to 1500 cm^{-1} is specific for amide-II bands, which is due to N-H bending vibrations.

There was a single prominent peak at 666.5 cm^{-1} in both the leaf extracts studied. This peak was fragmented and shifted in the silver and gold nanobioconjugate formation as evidenced in their IR spectra by the presence of two minor peaks at 1651 cm^{-1}, 1527 cm^{-1} with a single major peak at 1735 cm^{-1} in AgW and two minor peaks at 1643 cm^{-1}, 1527 cm^{-1} with a single major peak at 1735 cm^{-1} in AuW.

Two minor peaks were observed at 1527 cm^{-1}, 1620 cm^{-1} and a major peak at 1735 cm^{-1} in AgB. A single major peak at 1735 cm^{-1} was observed in AuB. This single major peak at 1735 cm^{-1} was common in all the four nanobioconjugates studied. There was a major peak at 1026 cm^{-1} and 1018 cm^{-1} in unconjugated WL and BL respectively. There was a slight shift and intensity decrease in these major peaks along with a number of additional minor peaks, indicating their role in nanobioconjugate formation and stabilization of both silver and gold nanobioconjugates. Another interesting feature was that the amide I band was shifted slightly in all the four the nanobioconjugates studied.

Figure 4.13

FTIR spectra of methanolic extract of *Clitoria ternatea* leaves bearing blue flowers (B) and their silver (AgB) and gold (AuB) nanobioconjugates

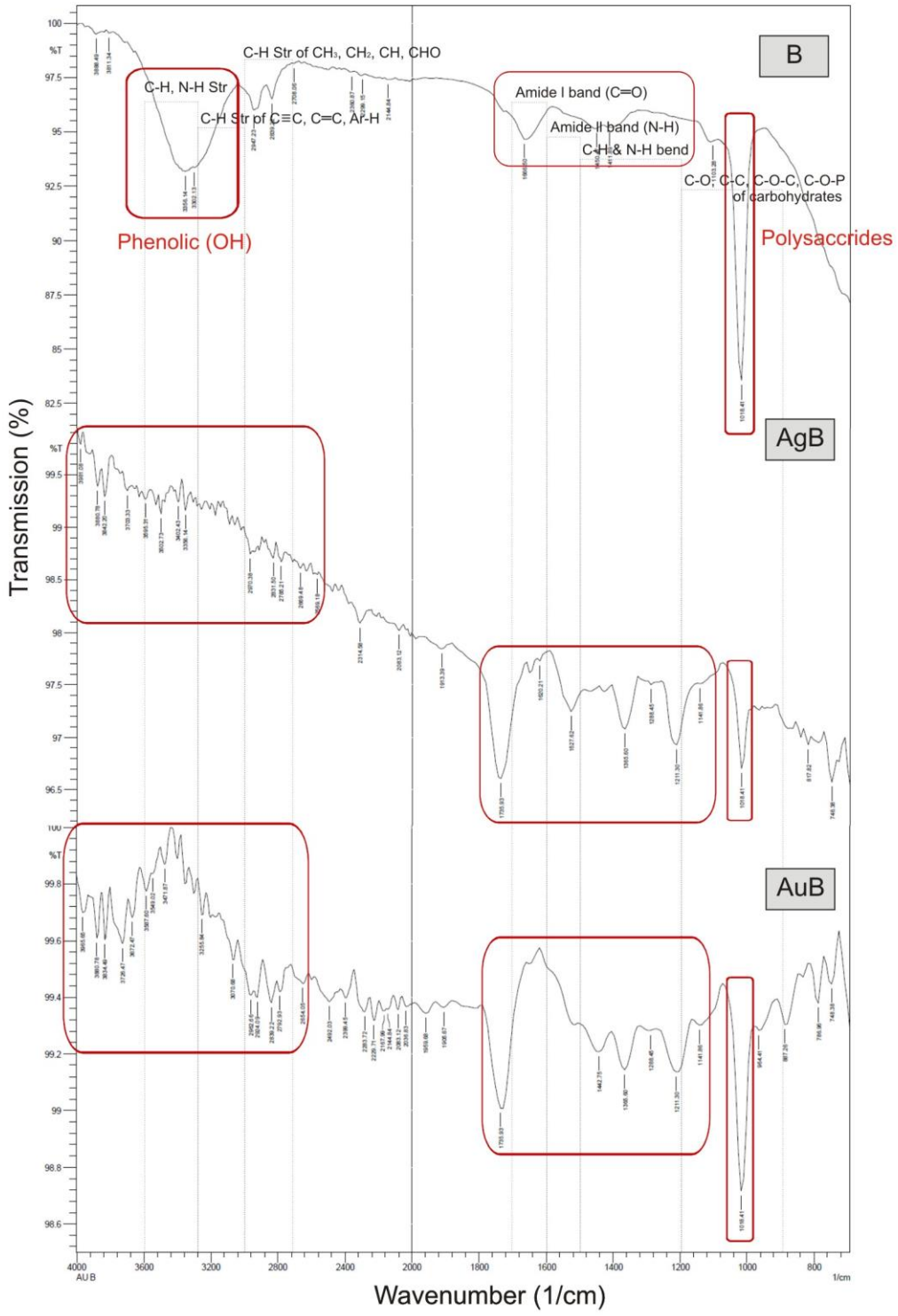

Figure 4.14

FTIR spectra of methanolic extract of *Clitoria ternatea* leaves bearing white flowers (W) and their silver (AgW) and gold (AuW) nanobioconjugates

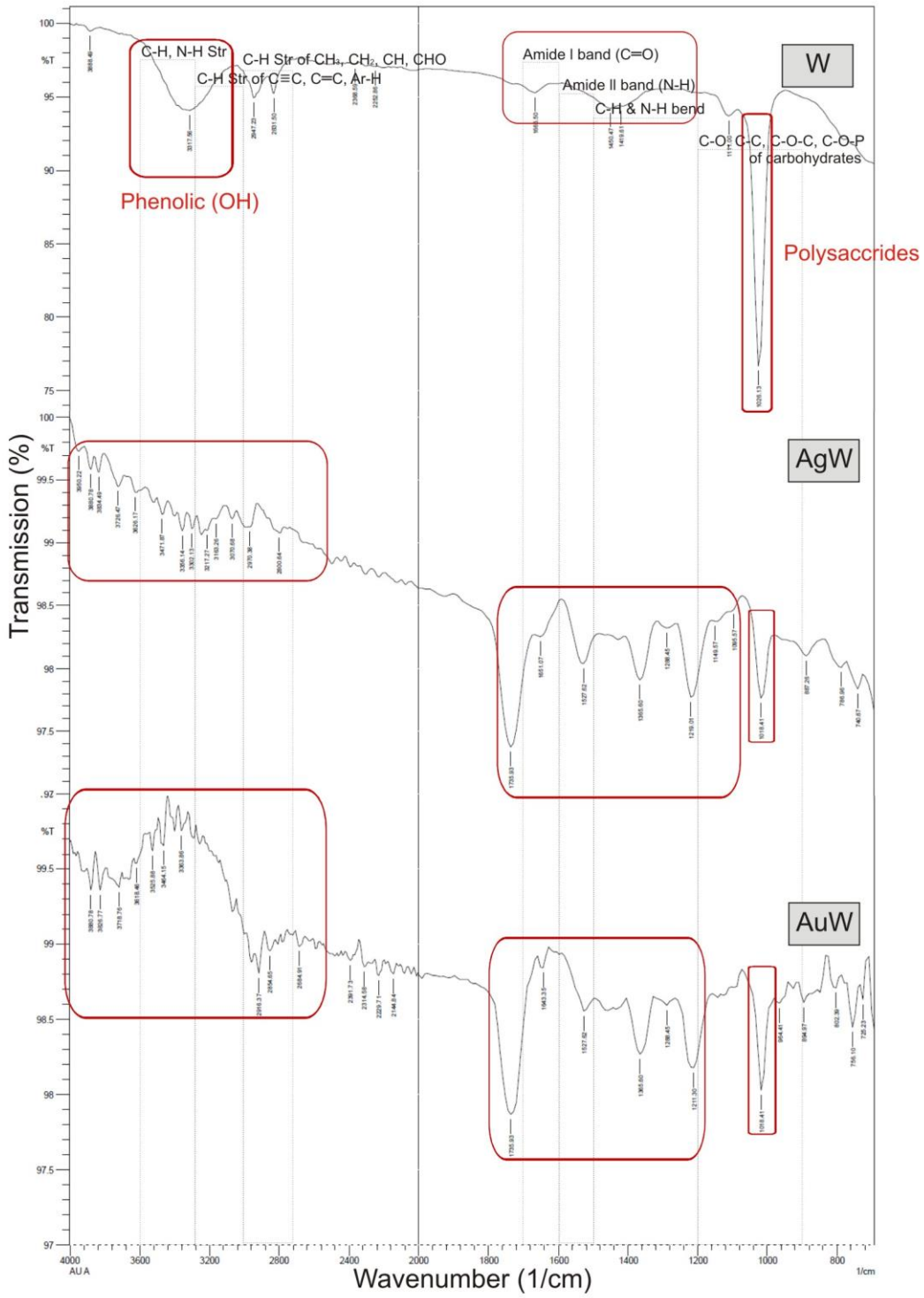

The bands in the 1500 cm^{-1} and 1200 cm^{-1} region arise mainly from the C-H bending vibrations of CH_3, CH_2 and CH functional groups. There were three minor peaks between 1500 cm^{-1} and 1200 cm^{-1}. Information on phosphodiester functional groups can be obtained in the region between 1250 cm^{-1} and 1200 cm^{-1} which corresponds to > P = O asymmetric stretching frequencies. In the present study, both the silver and gold nanobioconjugates showed an absorption band in this region, which is possibly due to P = O asymmetric stretching vibrations.

The region from 1200 cm^{-1} to 900 cm^{-1} are mainly dominated by a sequence of bands due to C-O, C-C, C-O-C and C-O-P stretching vibrations of polysaccharides as well as CH_3, CH_2 rocking modes. These groups mainly occur in carbohydrates and cellular polysaccharides. All the four nanobioconjugates, as well as their source leaf extracts, showed the polysaccharide band 1018 cm^{-1}. The intensity of this band decreased drastically after nanobioconjugates formation. Bands in this region showed additional peak formation and positional changes upon nanobioconjugate formation. Because of the complexity of the absorption of various cellular polysaccharides, specific assignments are rather difficult. Variation in spectral features attributes to hydroxyl, carbonyl, amino and phosphoryl groups to play a significant role in nanobioconjugate formation and stabilization.

Comparison of the IR data of silver and gold nanobioconjugates with their plant extracts provided direct evidence to show that hydroxyl, carbonyl, amino and phosphoryl functionalities played a significant role in synthesis and stabilization of silver and gold nanobioconjugates.

Yasmin *et al*. (2014) also performed a comparative FTIR spectral analysis of extracts of *H. rosasinensis* before and after the bioreduction of $HAuCl_4$ by the extracts and found a considerable shifts in the IR spectrum of AuNPs, showing that alkaloids or flavonoids would have adsorbed on the metal surface by the interaction with carbonyl/keto groups. Vetrivel *et al*. (2015) also used FTIR spectrum to calculate the various functional groups present in the NPs.

Arunachalam *et al*. (2013) explored FTIR to figure out the interaction of AgNPs with phytochemicals of *M. umbellatum*, and reported that the amide groups tended to form stronger bonds with the Ag atoms, breaking most of the H bonds between the N–H groups and leading to narrowing and blue shifts in the amide bond, indicating that the *M. umbellatum* proteins adsorb as a layer over the green-synthesized AgNPs, which stabilizes them. Krithiga *et al*. (2015) used FTIR spectrum to identify the possible biomolecules responsible for the capping and efficient stabilization of the silver nanoparticles synthesized by the aqueous leaf extracts of *Clitoria ternatea* and *Solanum nigrum*, and reported that several functional groups were identified in the FTIR spectrum of AgNPs from the aqueous leaf extracts of *C. ternatea*. Lakshmi *et al*. (2015) have reported the phytochemical screening and FTIR analysis of *C. ternatea* leaves and found similar results.

D'Souza *et al*. (2008) have reported that the FTIR pattern of marine brown alga (*Padina tetrastromatica*) grown in two different environmental conditions namely natural seawater and in seawater supplemented with cadmium showed variation in spectral features suggesting that cadmium ions bind to hydroxyl, amino, carbonyl and phosphoryl functionalities. Mollick *et al*. (2015) studied AgNPs of *A. esculentus* (L.) pulp extracts, and showed that different phytochemicals such as vitamins and proteins play an important role in the reduction of metal ions and the stabilization of the NPs.

In corroboration with the studies quoted above, our results also show that the functional groups present in the methanolic leaf extracts of *Clitoria ternatea* bearing blue and white flowers are involved in the bioconjugation with silver and gold, to form NPs. These observations also indicate the stability of the nanobioconjugates, as several functional groups are involved in the interaction. This was also confirmed by recording the zeta potential, as given below.

4.4.6 Zeta potential:

Long term stability of the nanobioconjugates is predicted through its zeta potential. It is a technique for determining the surface charge of nanoparticles in solution (colloids). In the present study, the zeta potential of the four types of nanobioconjugates synthesized (AgB, AgW, AuB and AuW) were studied. The results are depicted in Figure 4.15 (AgB and AgW) and Figure 4.16 (AuB and AuW) respectively. The zeta potential values of all the synthesised nanobioconjugates were well within the stable range (-11.8 to -8.56 mV), with a slight shift to the negative side, indicating an overall negative charge on the NPs. This showed that the nanobioconjugates synthesized were stable and potentially having longer shelf-life.

Poly dispersity index of each sample was also recorded alongside and are listed in Table 4.2. All the four nanobioconjugates showed polydispersity index values to be <0.4, indicating that the nanobioconjugates are well-dispersed without aggregation. Higher values have been indicated to have less homogeneous nanoparticle size distribution (Al-Quadeib *et al*., 2015).

Table 4.2

PDI of silver and gold nanobioconjugates

Types of leaves	AgNPs	AuNPs
Blue	0.328	0.276
White	0.261	0.394

AgNP aggregation studied through chemical reduction of silver nitrate in the presence of sodium borohydride (reducing agent) and sodium citrate (capping agent) by changing the amount of reducing agent along the reaction showed that the zeta potential and pH values had a strong influence on AgNP formation (Oliveira and Cardoso, 2014). Padalia *et al*. (2014) studied the stability of *T. erecta* flower AgNPs using zeta potential value and found a negative value (-27.63mV) suggesting that the surface of the NPs was negatively charged that dispersed in the medium.

Figure 4.15

Zeta potential of silver nanobioconjugates synthesized from *Clitoria ternatea* leaves bearing blue (AgB) and white (AgW) flowers

a) Silver nanobioconjugates of blue variety (AgB)

		Mean (mV)	Area (%)	St Dev (mV)
Zeta Potential (mV): -11.8	Peak 1:	-11.8	100.0	3.89
Zeta Deviation (mV): 3.89	Peak 2:	0.00	0.0	0.00
Conductivity (mS/cm): 0.0503	Peak 3:	0.00	0.0	0.00
Result quality : Good				

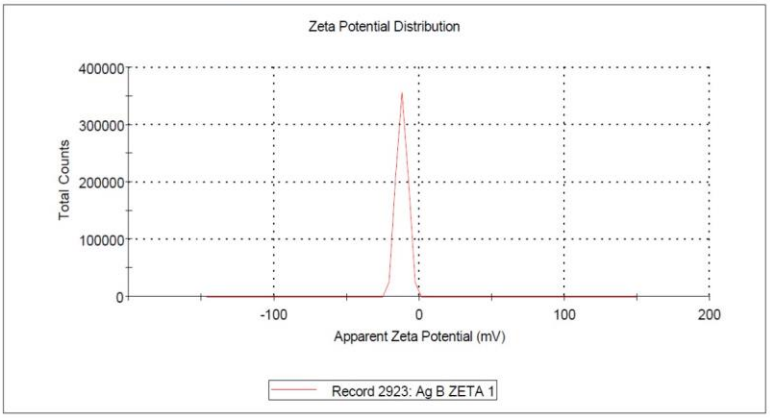

b) Silver nanobioconjugates of whitevariety (AgW)

		Mean (mV)	Area (%)	St Dev (mV)
Zeta Potential (mV): -10.7	Peak 1:	-10.7	100.0	11.3
Zeta Deviation (mV): 11.3	Peak 2:	0.00	0.0	0.00
Conductivity (mS/cm): 0.0665	Peak 3:	0.00	0.0	0.00
Result quality : Good				

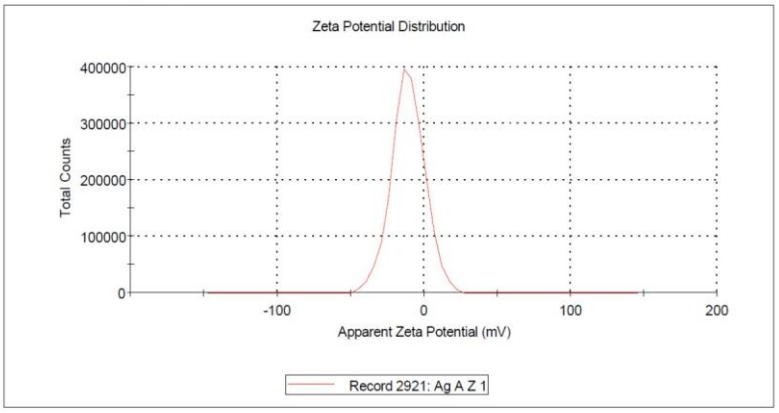

Figure 4.16

Zeta potential of gold nanobioconjugates synthesized from *Clitoria ternatea* leaves bearing blue (AuB) and white (AuW) flowers

a) Gold nanobioconjugates of blue variety (AuB)

		Mean (mV)	Area (%)	St Dev (mV)
Zeta Potential (mV): -10.7	Peak 1:	-10.7	100.0	11.3
Zeta Deviation (mV): 11.3	Peak 2:	0.00	0.0	0.00
Conductivity (mS/cm): 0.0665	Peak 3:	0.00	0.0	0.00
Result quality : Good				

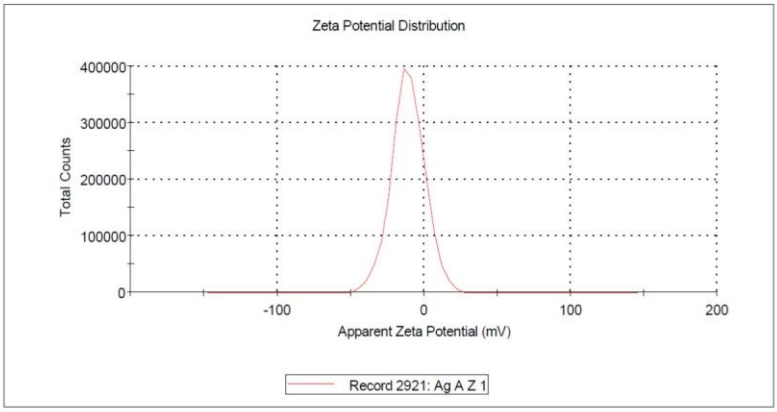

b) Gold nanobioconjugates of white variety (AuW)

		Mean (mV)	Area (%)	St Dev (mV)
Zeta Potential (mV): -10.3	Peak 1:	-10.3	100.0	3.84
Zeta Deviation (mV): 3.84	Peak 2:	0.00	0.0	0.00
Conductivity (mS/cm): 0.0731	Peak 3:	0.00	0.0	0.00
Result quality : Good				

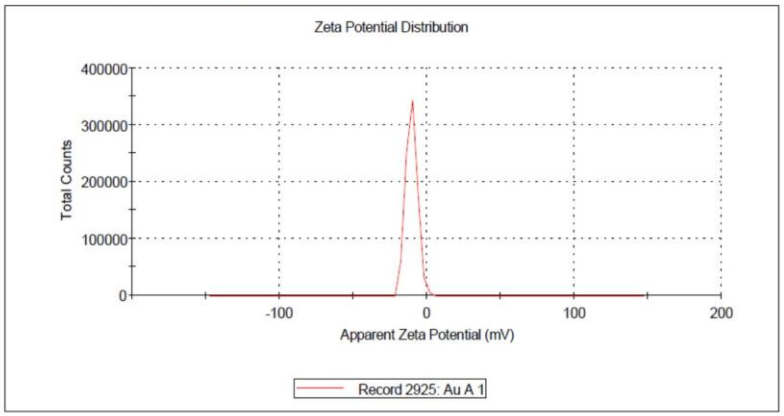

Tomaszewska *et al*. (2013) studied the size and size distribution of artificially prepared polydisperse silver nanoparticles colloids and found polydispersity index for monodisperse AgNPs smaller than 0.140. Ristig *et al*. (2015) prepared alloyed silver-gold NPs in nine different metal compositions with silver/gold molar ratio, ranging from 90:10 to 10:90 and found polydispersity index between 0.1 and 0.3, confirming a good degree of monodispersity. Cardoso *et al*. (2014) synthesized AgNPs stabilized with type I collagen (AgNPcol) to build a nanomaterial with biological utility, characterized in terms of particle size, zeta potential, and polydispersity index (PDI) and found a positive potential, between 0.40 and 0.77, for all AgNPcols.

The results of the second phase of the study showed that all the four NPs, namely, silver and gold particles synthesized from the leaf extracts of *Clitoria ternatea* bearing blue and white flowers were spherical in shape ranging in size from 10.4-46.2nm, which is well within the size range fixed for any particle to be termed as a nano (<100nm). The EDX profile showed the typical peak pattern of silver, gold and additional peaks that corresponded to the chemical elements of organic matter. These patterns clearly demonstrated that effective conjugation between silver and gold the biomaterial had occurred, resulting in the synthesis of bioactive nanobioconjugates respectively. The XRD patterns of the nanobioconjugates confirm the presence of silver, gold and organic material and crystalline nature of it. Comparison of IR data of silver and gold nanobioconjugates with their plant extracts shows the hydroxyl, carbonyl, amino and phosphoryl functionalities play a significant role in the synthesis and stabilization of nanobioconjugates. Zeta potential values of the synthesized nanobioconjugates were well within the stable range, showing that they were stable and potentially having longer shelf-life. Poly dispersity index of all nanobioconjugates were found to be <0.4 indicating they are homogenously distributed.

Thus, all the tests done for the characterization of nanobioconjugates confirmed the successful synthesis of ideal silver and gold

nanobioconjugates. In the next phase they were assessed for their bioactive nature.

PHASE III

Nanoparticles exhibit unique size-dependent physical and chemical properties that can be advantageous in the delivery of drugs, making advantages over chemical penetration enhancers such as sustained drug release for a prolonged period of time and protection of encapsulated materials from chemical degradation (Desai *et al*., 2010). In order to test whether such properties of the synthesized nanobioconjugates influenced the bioactivity, the third phase was dedicated to assess the bioactivity and biocompatibility of the prepared nanobioconjugates *in vitro*, in comparison with the respective extracts alone.

4.5 ASSESSMENT OF THE BIOACTIVITY OF NANOBIOCONJUGATES:

The silver and gold nanobioconjugates synthesized from *Clitoria ternatea* were assessed for their bioactivity against clinical isolates of bacteria and inflammation by *in vitro* methods.

4.5.1 Antibacterial activity of the nanobioconjugates:

The antibacterial activity of the silver, gold nanobioconjugates and their plant extracts were determined by agar well diffusion method against *Escherichia coli* and *Staphylococcus aureus* as a representation of Gram negative and Gram positive organisms respectively. The activity of plant extracts and their nanoparticles against both Gram positive and Gram negative bacteria may be an indicative of the presence of broad spectrum antibiotic compounds.

4.5.1.1 Agar well diffusion method:

The antibacterial activity was assessed by measuring the diameter of the inhibition zone formed around the wells and are presented in Plates 5a

and 5b and Table 4.3. It can be observed from the tabulated values that, in the Gram negative organism (*E. coli*), both silver and gold nanobioconjugates of both the varieties of *Clitoria ternatea* were significantly more effective than their unconjugated extracts.

Among the two metals, gold nanobioconjugates showed wider zones of inhibition and among the flower varieties, the leaves of white flower bearing plants exhibited better antibacterial effect. The effect of the gold nanobioconjugates of white variety (AuW) showed a zone of inhibition on par with the standard antibiotic, ampicillin.

In the Gram positive organism (*S. aureus*), though a zone of inhibition was observed in all the samples tested, the silver nanobioconjugates were not significantly effective over their respective unconjugated extracts in both the varieties. However, the gold nanobioconjugates of both the varieties (AuB and AuW) showed significantly higher bactericidal effect, which were comparable to that of the standard antibiotic, ampicillin.

Table 4.3

Antibacterial activity of leaf extracts of *Clitoria ternatea* bearing blue and white flowers and their silver and gold nanobioconjugates against *E. coli* and *S. aureus* by agar-well diffusion method

Organism	Zone of Inhibition (mm)						
	BL	**WL**	**AgB**	**AgW**	**AuB**	**AuW**	**Amp**
E. coli	21 ± 0.5^{a}	22 ± 0.5^{a}	29 ± 0.05^{c}	35 ± 0.5^{d}	$\mathbf{36\pm0.5^{e}}$	$\mathbf{37\pm0.05^{f}}$	39 ± 0.05^{g}
S. aureus	29 ± 0.05^{a}	31 ± 0.5^{b}	28 ± 0.05^{c}	32 ± 0.05^{d}	$\mathbf{35\pm0.05^{e}}$	$\mathbf{36\pm0.5^{f}}$	37 ± 0.05^{g}

Values are mean ± SD of six samples in each group

$^{a-g}$ Mean values with in a row no common superscript differ significantly at 5% by DMRT

Plate 4.7

a) Antibacterial activity of methanolic leaf extracts of *Clitoria ternatea* bearing blue and white flowers and their silver and gold nanobioconjugates against *E. coli* by agar-well diffusion method

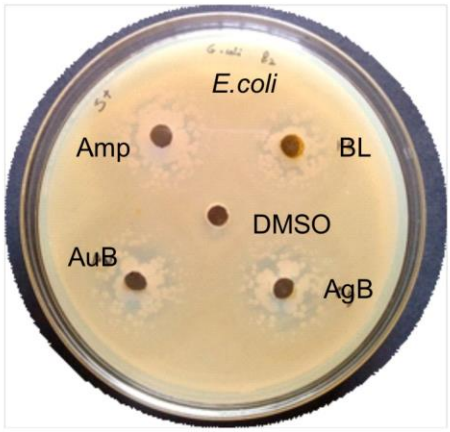

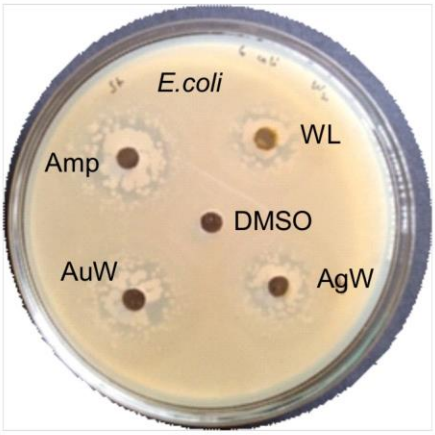

b) Antibacterial activity of methanolic leaf extracts of *Clitoria ternatea* bearing blue and white flowers and their silver and gold nanobioconjugates against *S. aureus* by agar-well diffusion method

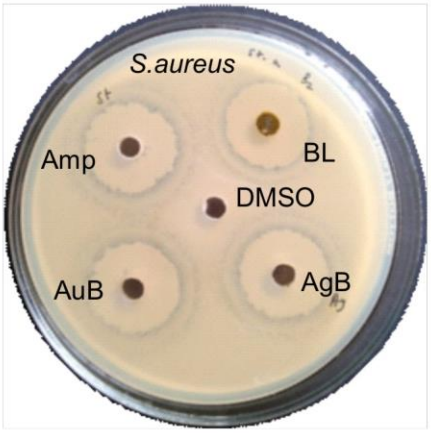

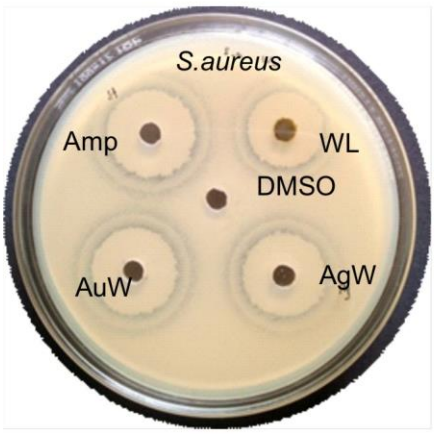

Amp- ampicillin; BL-blue leaf extract; WL- white leaf extract;
AuB- blue gold nanobioconjugates; AgB- blue silver nanobioconjugates;
AuW- white gold nanobioconjugates; AuB- blue gold nanobioconjugates;
DMSO- dimethyl sulfoxide

Thus, these observations confirmed that leaf extracts possess antibacterial components against both Gram positive and Gram negative organisms, which activity can be effectively enhanced by preparing silver and gold conjugated forms. The gold nanobioconjugates were more effective in this regard.

Babu *et al*. (2015) studied the antibacterial activity of silver nanoparticles incorporated in acrylic resin using agar well diffusion method and found that the resin matrix shows antibacterial property without affecting its compressive strength. Zhou *et al*. (2012b) also investigated the antibacterial effects of citrate Ag and Au NPs on *Bacillus Calmette-Guérin* and *Escherichia coli* and suggested that these NPs have potential applications as anti-TB compounds.

Ravikumar *et al*. (2012) investigated the *in vitro* antibacterial activity of five metal oxide nanoparticles namely, Al_2O_3, Fe_2O_3, CeO, ZrO_2 and MgO, against urinary tract infectious bacterial pathogens, namely *Pseudomonas* sp., *Enterobacter* sp., *Klebsiella* sp., *E. coli*, *Proteus morganii*, using agar well diffusion method and recorded maximum antibacterial activity in Al_2O_3 NPs.

Kalpana *et al*. (2014) biosynthesized AgNPs with *Torreya nucifera* and found the biosynthesized NPs were highly effective against *Salmonella typhimurium*. Friedman *et al*. (2013) reported the antimicrobial and anti-inflammatory activity of chitosan-alginate NPs against *P. acnes* in a dose-dependent manner.

In our study also, the nanobioconjugates were more effective in eliciting an antibacterial response. The gold nanobioconjugates of both the varieties of *C. ternatea* exhibited the maximum response among all the samples tested.

4.5.1.2 Determination of minimum inhibitory concentration (MIC):

MIC was determined in all the samples, as the extracts and nanobioconjugates exhibited good antibacterial effect against the test organisms (Table 4.4). The MIC is the concentration at which a sharp decline in the absorbance value is recorded. In *E.coli*, the MIC of gold nanobioconjugates was 100mg and silver nanobioconjugates was 200mg. The MIC of the unconjugated leaf extracts was around 800mg, showing that the efficacy of both the nanobioconjugates was much better than the plant extracts.

Table 4.4

MIC of nanobioconjugates and methanolic leaf extracts of *Clitoria ternatea* bearing blue and white flowers

Organism	MIC (µg)					
	BL	**WL**	**AgB**	**AgW**	**AuB**	**AuW**
Escherichia coli	800	800	200	200	100	100
Staphylococcus aureus	800	800	400	400	200	200

In *S. aureus*, the MIC of silver nanobioconjugates was 400mg and gold nanobioconjugates was 200mg. The MIC of the unconjugated leaf extracts was around 800mg, showing that the efficacy of both the nanobioconjugates was much better than the plant extracts.

Devienne and Raddi (2002) reported the antimicrobial effect of Paepalantine against *S. aureus*, which was similar to chloramphenicol. Malabadi *et al*. (2012) have recorded higher the antibacterial activity of AgNPs synthesized from the whole plant extracts of *Clitoria ternatea* (L.) against Gram positive bacteria, *Bacillus subtilis* and *Staphylococcus aureus* and Gram negative bacteria, *Escherichia coli* and *Klebsiella pneumonia*. Sen and Batra (2012) examined the antimicrobial efficiency of the leaf extracts of *Melia azedarach* L. against eight human pathogens, and found them to be effective against all organisms.

Figure 4.17

MIC of silver and gold bionanoconjugates and methanolic leaf extracts of *Clitoria ternatea* bearing blue and white flowers against *E. coli*

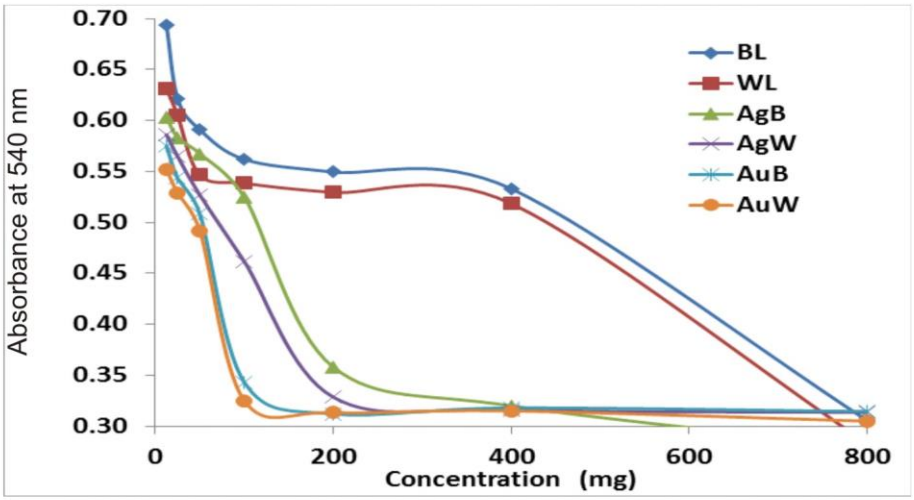

Figure 4.18

MIC of silver and gold bionanoconjugates and methanolic leaf extracts of *Clitoria ternatea* bearing blue and white flowers against *S. aureus*

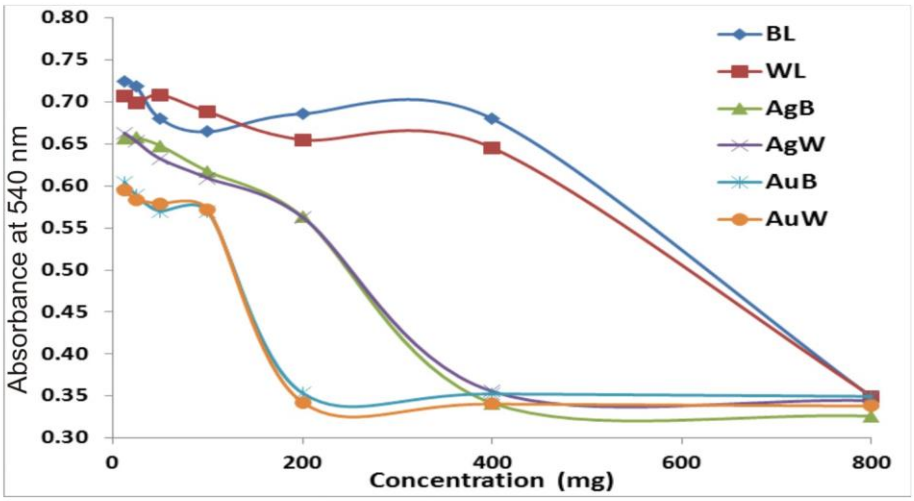

The values are mean ± SD of triplicates
BL- blue leaf extract; WL- white leaf extract;
AgB- silver nanobioconjugates from blue variety;
AgW- silver nanobioconjugates from white variety;
AuB- gold nanobioconjugates from blue variety;
AgW- gold nanobioconjugates from white variety

4.5.2 Assessment of *in vitro* anti-inflammatory activity:

Inflammation is the reaction of living tissues to injury, infection or irritation. Lysosomal enzymes released during inflammation produce a variety of disorders, which lead to tissue injury by damaging the macromolecules and causing lipid peroxidation of membranes, which are assumed to be responsible for certain pathological conditions like heart attacks, septic shocks and rheumatoid arthritis. The extra cellular activity of these enzymes is said to be related to acute or chronic inflammation. Stabilization of lysosomal membrane is important in limiting the inflammatory response by inhibiting the release of lysosomal constituents of activated neutrophil such as bactericidal enzymes and proteins, which cause further tissue inflammation and damage upon extra cellular release or by stabilizing the lysosomal membrane (Chippada *et al*., 2011; Kumar *et al*., 2011).

In the present study, the *in vitro* anti-inflammatory activity of the extracts and their Ag and Au NPs were evaluated by Human Red Blood Cell (HRBC) membrane stabilization, protein denaturation, heat induced hemolysis and proteinase inhibition activities and the results are documented below.

4.5.2.1 HRBC membrane stabilization activity:

HRBC or erythrocyte membrane is analogous to the lysosomal membrane and its stabilization implies that the extract or drug tested may as well stabilize lysosomal membranes. Stabilization of HRBC by hypotonicity induced membrane lysis can be taken as an *in vitro* measure of anti-inflammatory activity of the drugs or plant extracts (Chippada *et al*., 2011).

HRBC membrane stabilization activities of the Ag and Au NPs synthesized were performed and per cent lysis was presented in Table 4.5. The per cent stabilization was calculated from it and showed in Figure 4.19. AuNPs inhibited the hypotonic solution-induced haemolysis effectively followed by AgNPs. The protection of gold nanobioconjugates was comparable with that of standard drug aspirin indicating that the nanobioconjugates were biologically compactable.

Table 4.5

Effect of lysis of HRBC by silver and gold nanobioconjugates from methanolic leaf extracts of *Clitoria ternatea*

Sample	% lysis
Positive control	100
AgB	21.20±1.48
AgW	22.82±1.28
AuB	19.52±1.45
AuW	18.32±1.35
Aspirin	10.19±1.31

The values are mean ± SD of triplicates

Pant *et al*. (2012) have reported the anti-inflammatory activities of different extracts of leaves of *Anthracephalus cadamba*, as the HRBC membrane stabilizing effect. Sanadhya et al. (2014) observed a concentration dependent HRBC membrane stabilizing activity with increasing concentration of the methanolic extracts of *Costus speciosus* leaves.

Figure 4.19

Effect of silver and gold nanobioconjugates from methanolic leaf extracts of *Clitoria ternatea* on stabilization of HRBC membrane

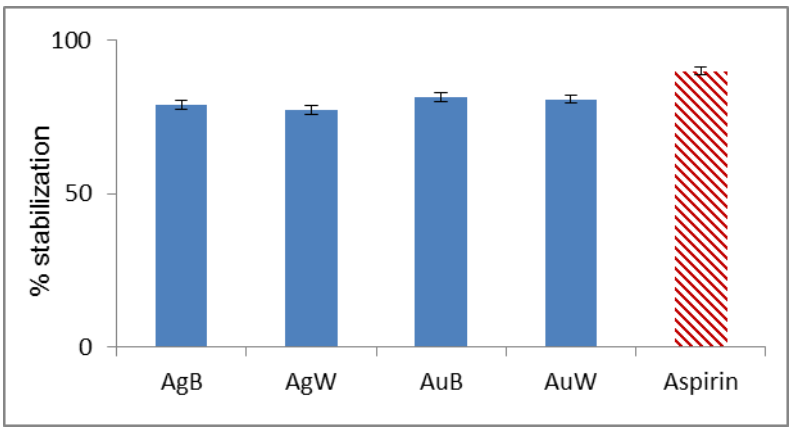

The values are mean ± SD of triplicates

Chatter *et al*. (2011) used HRBC membrane lysis and showed that the red algae-derived natural molecule neorogioltriol, was able to show inhibition in a concentration- and time-dependent manner. The membrane stabilizing activity of the fruit extract of *P. cereifera* was assessed using heat-induced hemolysis of mice erythrocyte and was demonstrated to have significant anti-inflammatory activity (Md.Reyad-ul-Ferdous *et al.*, 2015). Reshma *et al*. (2014) studied the *in vitro* anti-inflammatory activity of the leaves of *Aegle marmelos* and *Ocimum sanctum* using protease inhibition activity, membrane stabilization and protein denaturation inhibition assays proving the ethnomedicinal claim of the medicinal properties of these selected plant drugs.

Our results also showed that the green synthesized silver and gold nanobioconjugates of *Clitoria ternatea* leaf extracts were able to inhibit the lysis and stabilized the HRBC membrane effectively. The gold nanobioconjugates were better in this than their silver counterpart.

4.5.2.2 Heat Induced Hemolysis:

The inhibition of heat induced hemolysis can be taken as a measure of the anti-inflammatory activity (Sanadhya *et al*., 2014). The absorbance values were recorded and the percentage of hemolysis and its protection by methanolic leaf extracts and their silver and gold nanobioconjugates were calculated. The results are presented in Figure 4.20.

Gold nanobioconjugates inhibited the heat induced haemolysis more effectively than the silver nanobioconjugates. The protection by gold nanobioconjugates was comparable with that of standard drug aspirin. The white variety of *C. ternatea* exhibited better protection than the blue variety. None of the nanobioconjugates enhanced the heat induced hemolysis indicating that they are biologically compatible.

Figure 4.20

Effect of silver and gold nanobioconjugates of *Clitoria ternatea* against heat induced hemolysis

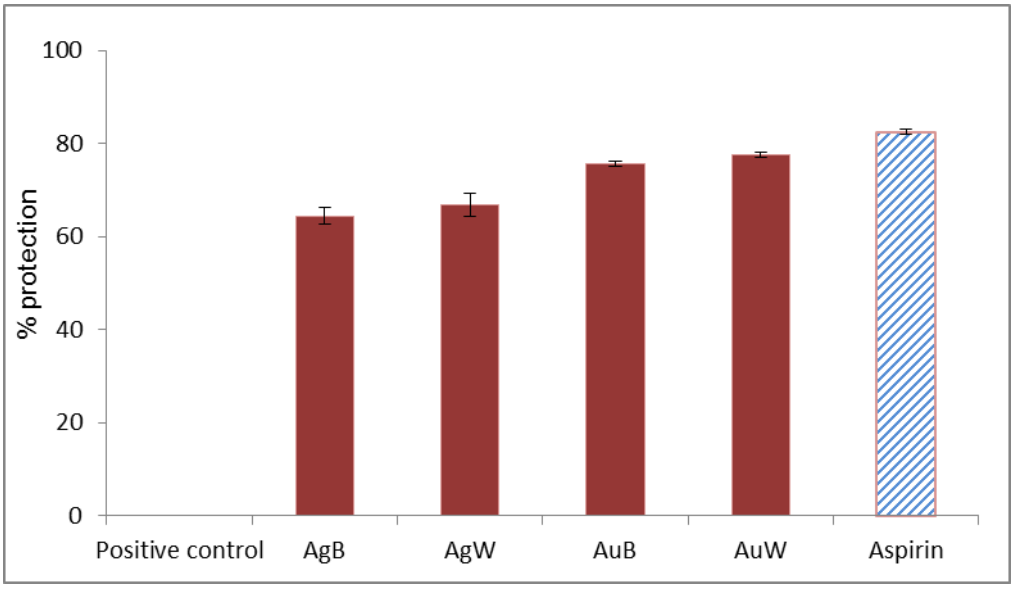

The values are mean ± SD of triplicates

Chandrappa *et al*. (2013) studied the *in vitro* anti-inflammatory activity of ethanol extract of stem of *Carmona retusa* by human red blood cell membrane stabilization method, heat induced hemolysis and proteinase inhibitory activity and reported the potential of the extracts against inflammation. In a study by Ranasinghe *et al.* (2012), *Carica papaya* L. leaf extracts, on investigation of their membrane stabilization properties, were shown to significantly reduce heat-induced hemolysis.

In our results, the nanobioconjugates protected the lysis of blood cells, suggesting that they do not exhibit any toxicity to the cells.

4.5.2.3 Protein denaturation assay:

Protein denaturation is implicated in inflammation (Opie, 1962). To assess the potential anti-inflammatory activity of the nanobioconjugates, the protein denaturation assay was performed and the results are presented in Figure 4.21. Denaturation of proteins is a well-documented cause of inflammation (Gupta *et al*., 2013).

In vitro anti-inflammatory activity of silver and gold nanobioconjugates synthesized from the methanolic leaf extracts of *Clitoria ternatea* bearing blue and white flowers was assessed by their ability to inhibit the protein denaturation. All the nanobioconjugates tested were able to inhibit the protein denaturation and gold nanobioconjugates inhibited the protein denaturation more effectively, followed by silver nanobioconjugates. The inhibition rendered by gold nanobioconjugates were comparable with that of the standard drug, aspirin.

Chandra *et al*. (2012) have shown a dose dependent *in vitro* anti-inflammatory effect of aqueous extract of coffee (*Coffea arabica*) as the inhibition of protein (albumin) denaturation. The anti-inflammatory activity of the extract of *C. violacea*, was reported using human red blood membrane stabilization and albumin denaturation method (Bougandoura *et al*., 2016).

Figure 4.21

Effect of silver and gold nanobioconjugates of *Clitoria ternatea* on protein denaturation

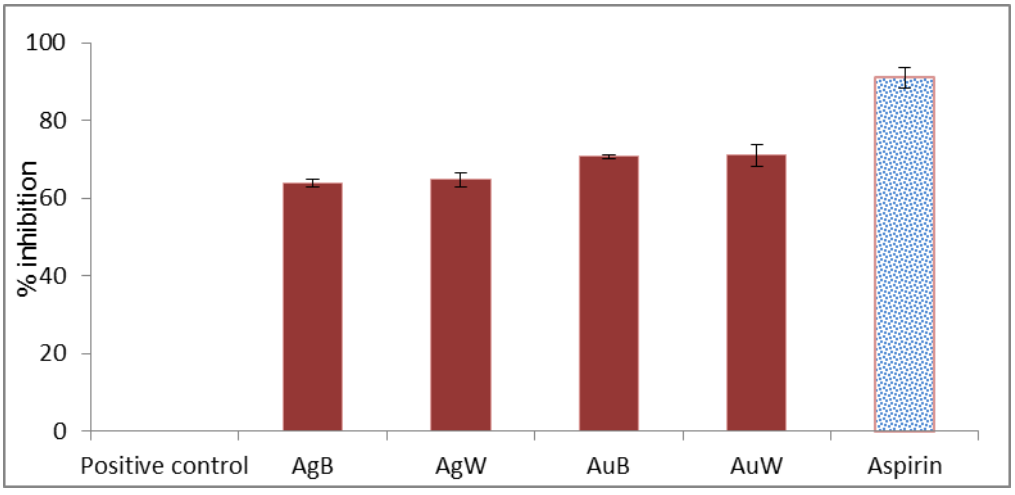

The values are mean ± SD of triplicates

Leelaprakash and Dass (2011) assessed the *in vitro* anti-inflammatory activity of methanol extract of *Enicostemma axillare* using membrane stabilization, albumin denaturation assay and proteinase inhibitory activity at different concentrations and reported that the methanol extracts of *E. axillare* can be a potential source of anti-inflammatory agents. Yu *et al*. (2016) also

used *in vitro* inflammation systems and proved that the ginsenoside Rc from *Panax ginseng* extracts possess good anti-inflammatory activity.

The present study also used the inhibition of protein denaturation as a tool to assess the *in vitro* anti-inflammatory activity of nanobioconjugates and the results showed that the nanobioconjugates are a good source of anti-inflammatory components.

4.5.2.4 Proteinase inhibitory activity:

Denaturation of proteins is a well-documented cause of inflammation (Gupta *et al*., 2013). *In vitro* anti-inflammatory activity of silver and gold nanobioconjugates synthesized from the methanolic leaf extracts of *Clitoria ternatea* bearing blue and white flowers were assessed by their proteinase inhibitory activity. All the nanobioconjugates tested were able to inhibit proteinase. Gold nanobioconjugates inhibited more effectively, followed by silver nanobioconjugates (Figure 4.22). The inhibition rendered by gold nanobioconjugates were comparable with that of the standard drug, aspirin.

Figure 4.22

Effect of silver and gold nanobioconjugates of *Clitoria ternatea* on proteinase activity

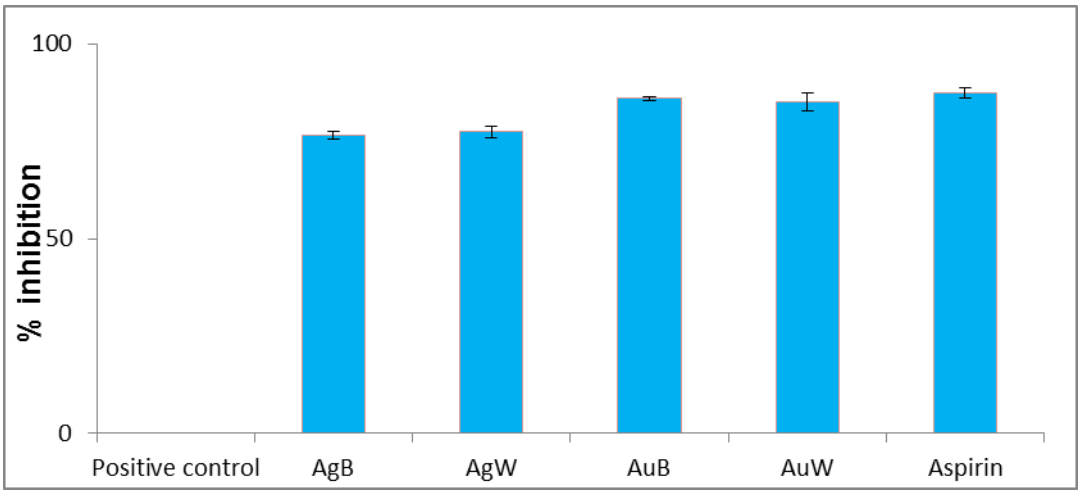

The values are mean ± SD of triplicates

Padmanabhan and Jangle (2012) evaluated the *in vitro* anti-inflammatory activity of herbal preparations of *Aloe vera*, *Bacopa monnieri*, *Moringa oleifera* and *Zingiber officinale* at different concentrations by membrane stabilization and protein denaturation and found dose dependent anti-inflammatory activity. Kata *et al*. (2016) proved that rosuvastatin enhanced the anti-inflammatory effect and inhibited pro-inflammatory functions in cultured microglial cells, using proteinase inhibition.

Murugan and Parimelazhagan (2013) used the different extracts of *Osbeckia parvifolia* for anti-inflammatory activities by protein denaturation and membrane stabilization assays and found that the whole plant could serve as a potential source for antioxidant and anti-inflammatory property from natural origin. Sakat *et al*. (2010) showed the methanolic extract of whole plant of *Oxalis corniculata* Linn. to have *in vitro* anti-inflammatory activity. Hamidpour *et al.* (2016) indicated the anti-inflammatory property of *Elaeagnus angustifolia* L.

In the present study, inhibition of proteinase activity was used as a tool to assess the *in vitro* anti-inflammatory activity of nanobioconjugates and the results showed that the nanobioconjugates of the plant *C. ternatea* are potential source of anti-inflammatory activity.

From the above results it is clear that the silver and gold nanobioconjugates of *C. ternatea* leaf extracts possess better bioactivity than their unconjugated extracts, further their biocompatibility was assessed to confirm their biosafety.

4.6 ASSESSMENT OF BIOCOMPATIBILITY:

In recent years, NPs have increasingly found practical applications in technology, research and medicine. The small particle size coupled with their unique chemical and physical properties is thought to contribute to their exploitable biomedical activities. Due to their small size and physical

resemblance to physiological molecules such as proteins, NPs possess the capacity to revolutionize medical imaging, diagnostics, therapeutics, as well as carry out functional biological processes. But these features may also underline their toxicity. Therefore, a detailed assessment of the factors that influence the biocompatibility and toxicity of nanobioconjugates is crucial for the safe and sustainable development of the emerging NPs.

Biocompatibility of any drug can be measured by analyzing its effect on blood (Chen *et al.*, 2012). For this, RBC lysis, blood clotting time, morphological changes of RBC and blood lymphocytes were studied.

4.6.1 Red blood cell lysis:

The biocompatibility of the silver and gold nanobioconjugates prepared were tested on RBCs isolated from healthy individuals. Along with test samples, water was also tested and fixed as 100%. The extent of hemolysis for all the extracts and nanobioconjugates were calculated relative to that of the water control (Figure 4.23). The extent of hemolysis was found to be <1% for all the samples tested, indicating that they were able to protect the cells against hemolysis, and are, therefore, safe for use in humans.

Figure 4.23

Effect of silver and gold nanobioconjugates synthesized from *Clitoria ternatea* leaves bearing blue and white flowers on hemolysis

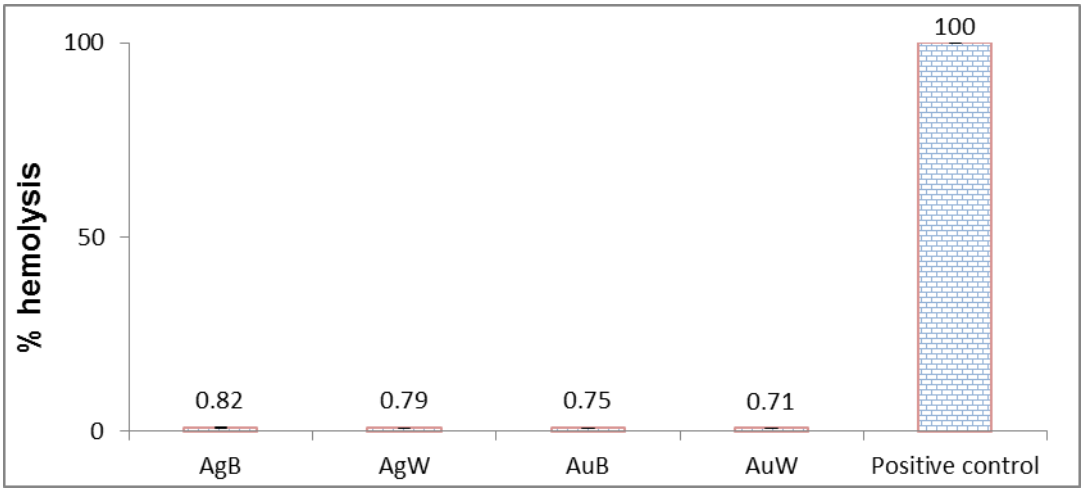

The values are mean ± SD of triplicates

4.6.2 Effect of silver and gold nanobioconjugates on whole blood clotting:

The effect of silver and gold nanobioconjugates prepared from the methanolic leaf extracts on whole blood clotting was assessed as a measure of toxicity. There were no significant differences observed in the any of the samples tested comparing with control saline group (Figure 4.24). This again confirms that the nanobioconjugates of *Clitoria ternatea* were safe and biocompatible.

Figure 4.24

Effect of silver and gold nanobioconjugates on whole blood clotting

The values are mean ± SD of triplicates

Ohkura *et al*. (2015) screened popular Chinese medicinal herbs for hemostatic activities *in vitro* and reported that the extracts shortened the clotting time. The gold nanoparticles of *Peltophorum pterrocarpum* extracts had anticoagulation activity (Raja *et al*., 2015). In our results, the silver and gold bionanoconjugates of *C. ternatea* do not influence the clotting time implying their biosafety.

4.6.3 Plasma re-calcification profile:

Kinetics of clotting process due to re-calcification can be monitored by this assay at different time points. The clotting process consists of both

intrinsic and extrinsic pathways, which ultimately lead to clot formation. The intrinsic cascade is initiated when blood contacts a surface, while the extrinsic pathway is initiated upon vascular injury which leads to exposure of tissue factor. The intrinsic clotting pathway suggests that a 'pro-coagulant stimulus', starting with the exposure of plasma to a test surface, potentiates a cascade of events that culminates in the release of thrombin (Factor IIa). In the progression of the intrinsic pathway of clot formation, calcium is involved as an activating factor. Therefore, plasma re-calcification profiles serve as a measure of the intrinsic coagulation system and can be used to investigate whether the blank nanobioconjugates surface would trigger this blood-biomaterial interaction (He *et al*., 2009).

The re-calcification clotting profiles and clotting rates of nanobioconjugates are shown in Figures 4.25, 4.26, 4.27 and 4.28. The absorbance increased as the plasma became more turbid, which suggests the formation of a clot. A rightward shift of the curve indicates an overall slower clot time; whereas a leftward shift of the curve indicates a faster clot time. Platelet poor plasma (PPP) without the addition of $CaCl_2$ served as a negative control, as it does not clot within the experimental time. The time required to reach half maximal absorbance (half-max time) was calculated as a measure of clotting time for each sample. All the four nanobioconjugates were found to have half-max ~ 6 minutes, which is well within the normal clotting time (2 to 6 minutes) indicating that the nanobioconjugates are non-toxic.

Nanobioconjugates having a less coagulative surface can be evidenced by a rightward shift in the curves, and the longest half-max time. More the re-calcification clotting profiles moved rightwards. Blood clotting time for thirty nine polymers have been studied among which nine did not to exhibit the desired blood compatibility (He *et al*., 2009). Leitao *et al*. (2013) assessed the hemocompatibility of the BC/PVA nanocomposite using whole blood clotting time, plasma re-calcification, hemolytic index and complement activation and reported its biocompatibility and suggested that it is suitable for

cardiovascular application. Sulfate derivative of *Capparis spinosa* L. fruits Sul-2B-2 had moderate effect on re-calcification time (Wang *et al*., 2012).

Coagulation properties of biodegradable chitosan-graft-polylactide copolymers were evaluated using hemolysis, plasma re-calcification, dynamic blood clotting and protein absorption assays and reported that the copolymers cause similar hemolysis ratio and plasma re-calcification time as polylactide (Wang *et al*., 2014).

In our study, all the four nanobioconjugates showed normal clotting time.

Figure 4.25

The plasma re-calcification profile of silver nanobioconjugates of *Clitoria ternatea* leaves bearing blue flowers

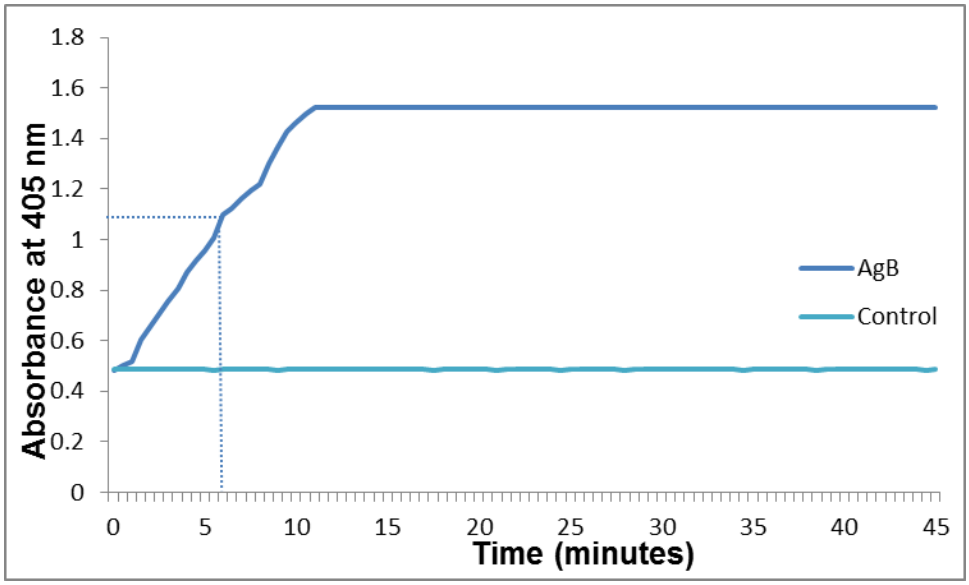

Figure 4.26

The plasma re-calcification profile of silver nanobioconjugates of *Clitoria ternatea* leaves bearing white flowers

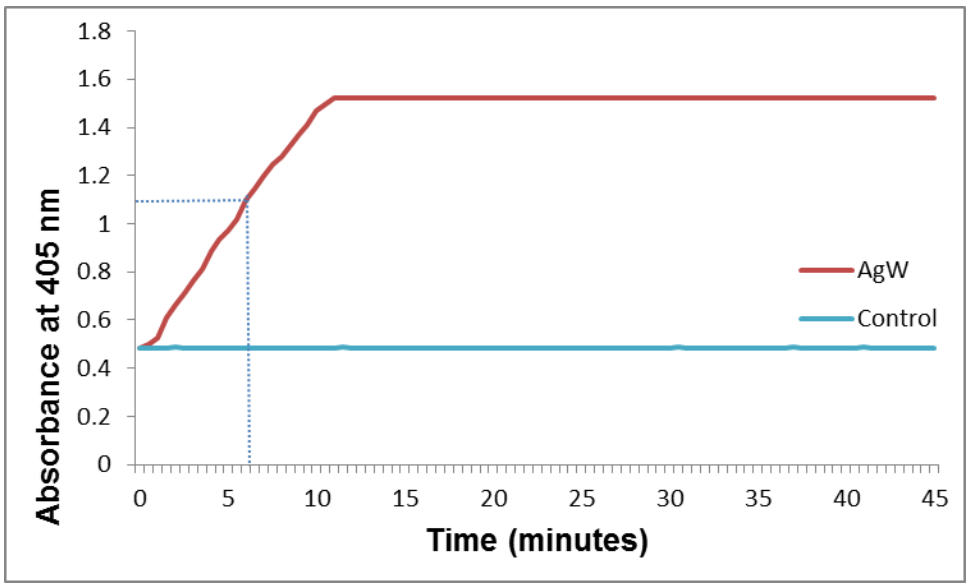

Figure 4.27

The plasma re-calcification profile of gold nanobioconjugates of *Clitoria ternatea* leaves bearing blue flowers

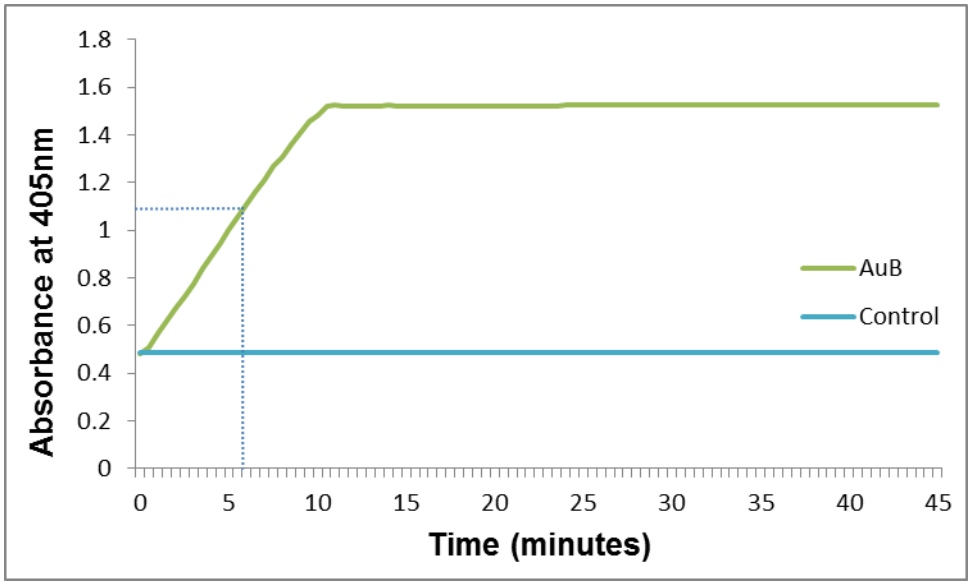

Figure 4.28

The plasma re-calcification profile of gold nanobioconjugates of *Clitoria ternatea* leaves bearing white flowers

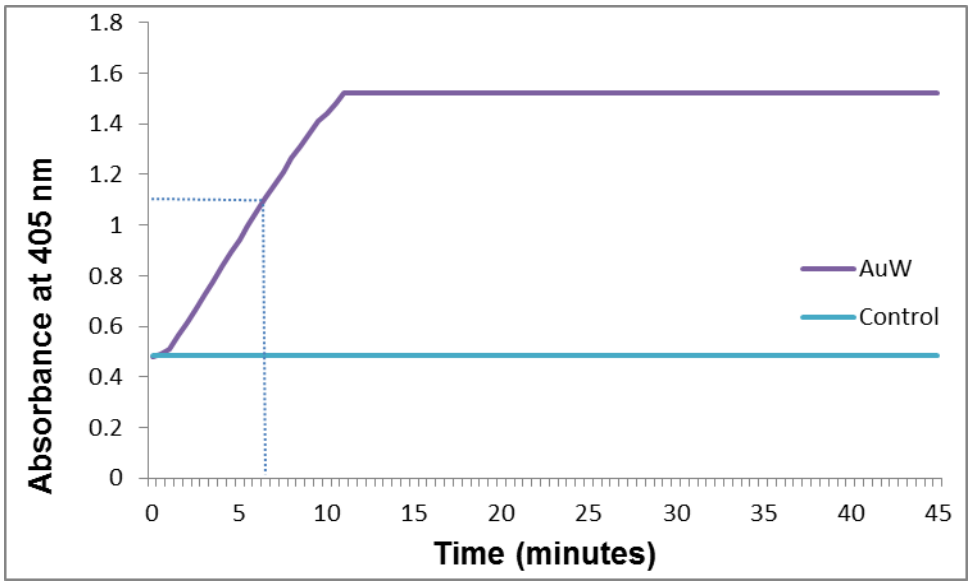

4.6.4 Red blood cell form and appearance in whole blood:

The appearance whole blood cell after incubation with nanobioconjugates (test samples), saline (negative control) and water (positive control) was utilized as a tool to find out the effect of it on blood cells. Maximum cell lysis was observed in the group treated with water. Absence of morphological changes (no lysis) is an indication that the nanobioconjugates are non-toxic to the blood cells (Plate 4.7).

Laloy *et al*. (2014) studied extent of hemolysis, morphological changes to blood cells and coagulation pattern of whole blood as a parmeters indicative of silver nanoparticles toxicity. Irrespective of the route of administration (oral or intravenous), nanoparticles enter the blood circulation and are then futher distributed in the body. The results showed that the nanobioconjugates were non-toxic to the cells, reiterating the results of other biocompatibility assays.

Plate 4.8

Effect of silver and gold nanobioconjugates on the morphology of human blood cells

Saline (Normal)

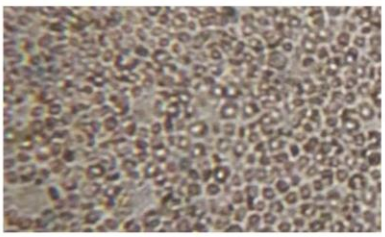

Water (Lysis)

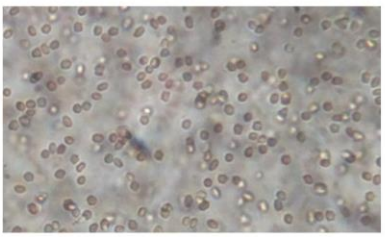

AgB

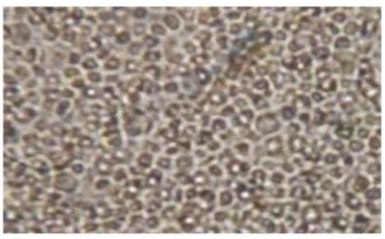

AgW

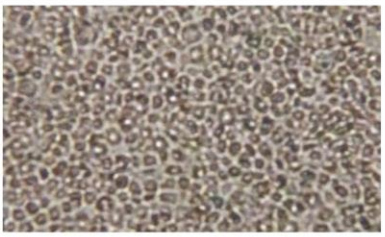

AuB

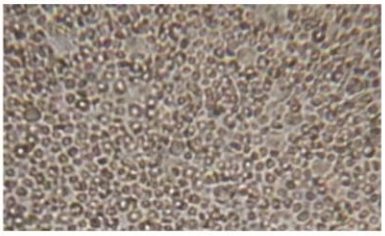

AuW

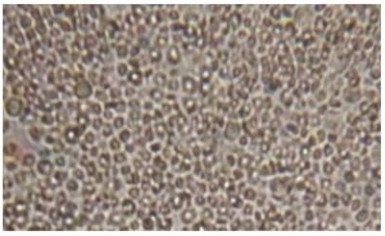

4.6.5 Assessment of drug release:

Biocompatibility and cytotoxicity continue to be two fundamental issues in using the bioconjugates as therapeutic and diagnostic tools (Uchiyama *et al*., 2014). The drug release kinetic profiles of the nanobioconjugates prepared from the methonolic leaf extracts of both the varieties were recorded from 0 hour upto 45 hours at one-hour intervals. Then after which a plateau occurred. From the Figures 4.29, 4.30, 4.31 and 4.32, it is clear that the nanoparticles released slowly upto 15-16 hours.

Razavilar and Choi (2012) reviewed the *in vitro* modeling of the release kinetics of hydrophobic drugs encapsulated by polymeric materials. Sethi *et al*. (2014) reported that drug release kinetics can affect the therapeutic efficacy of nanoparticle docetaxel and nanoparticle wortmannin *in vitro* and *in vivo* and demonstrated that a decrease in drug release kinetics can result in a decrease in the hepatotoxicity of cross linkable lipid shell nanoparticle of wortmannin.

Figure 4.29

Drug release profile of the silver nanobioconjugates of blue flowered variety

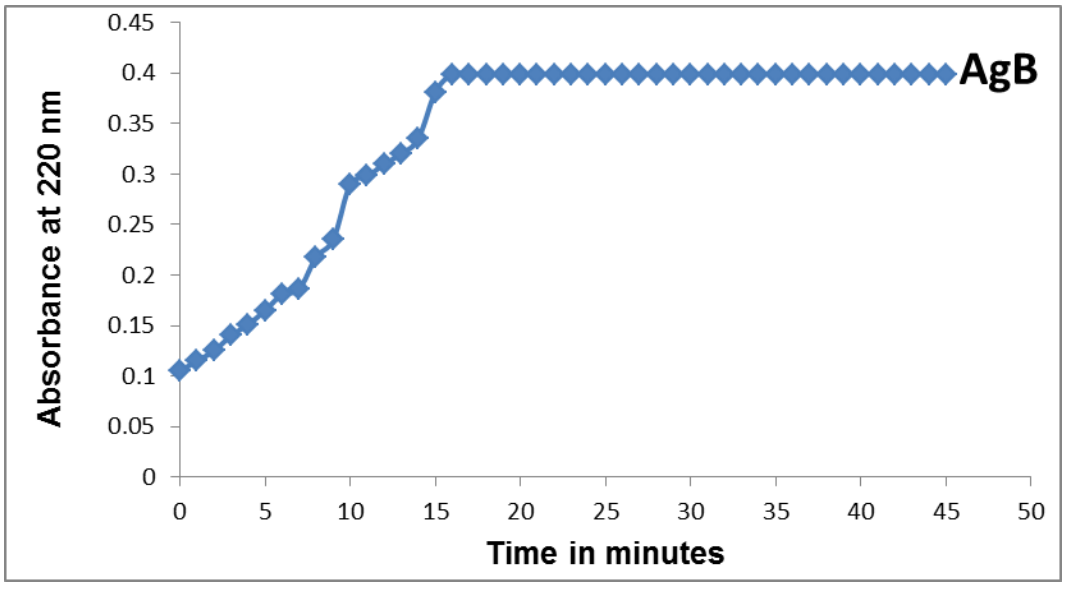

Figure 4.30

Drug release profile of the silver nanobioconjugates of white flowered variety

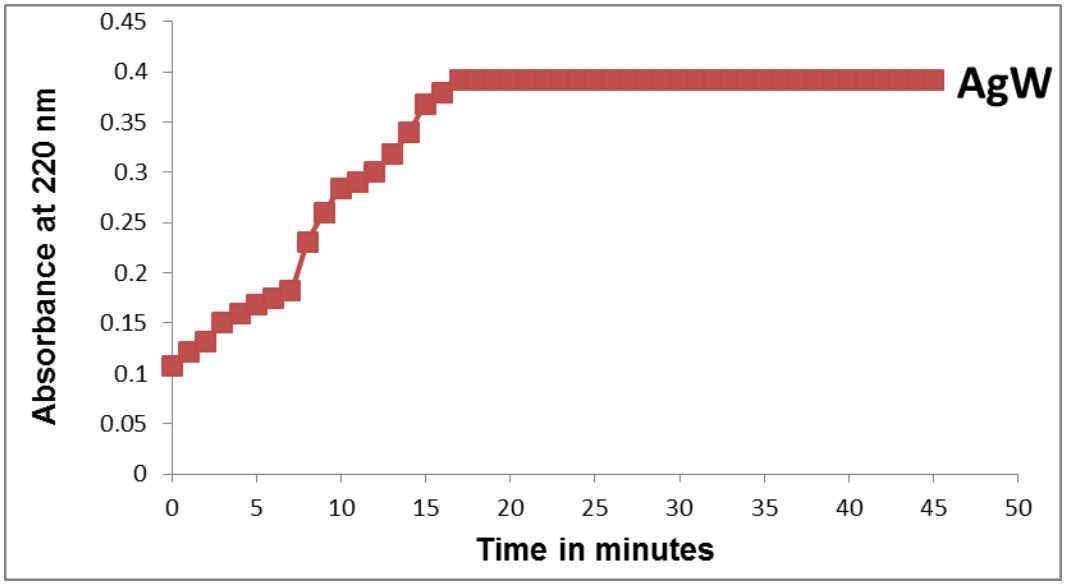

Figure 4.31

Drug release profile of the gold nanobioconjugates of blue flowered variety

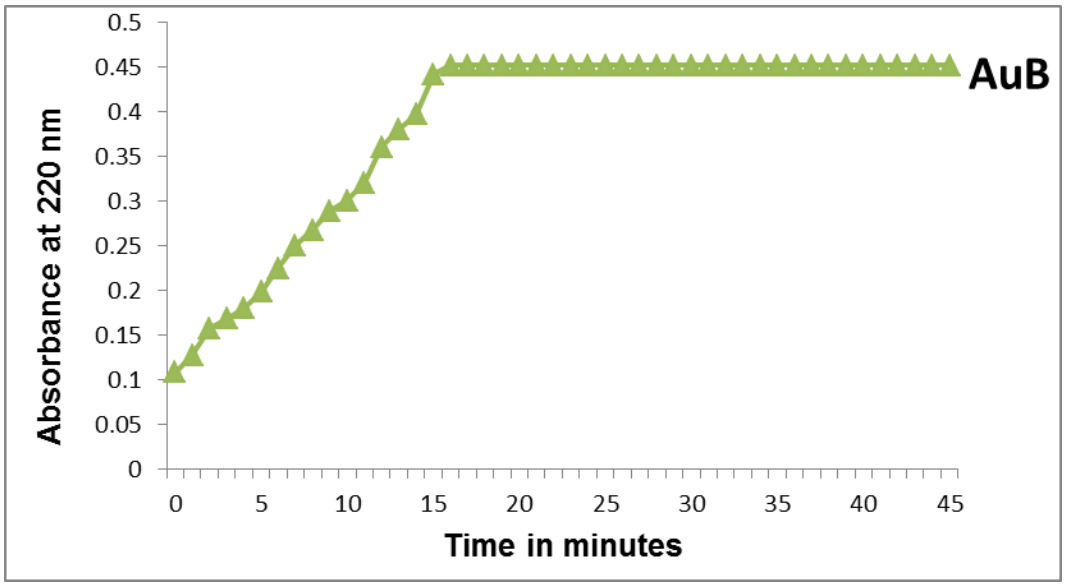

Figure 4.32

Drug release profile of the gold nanobioconjugates of white flowered variety

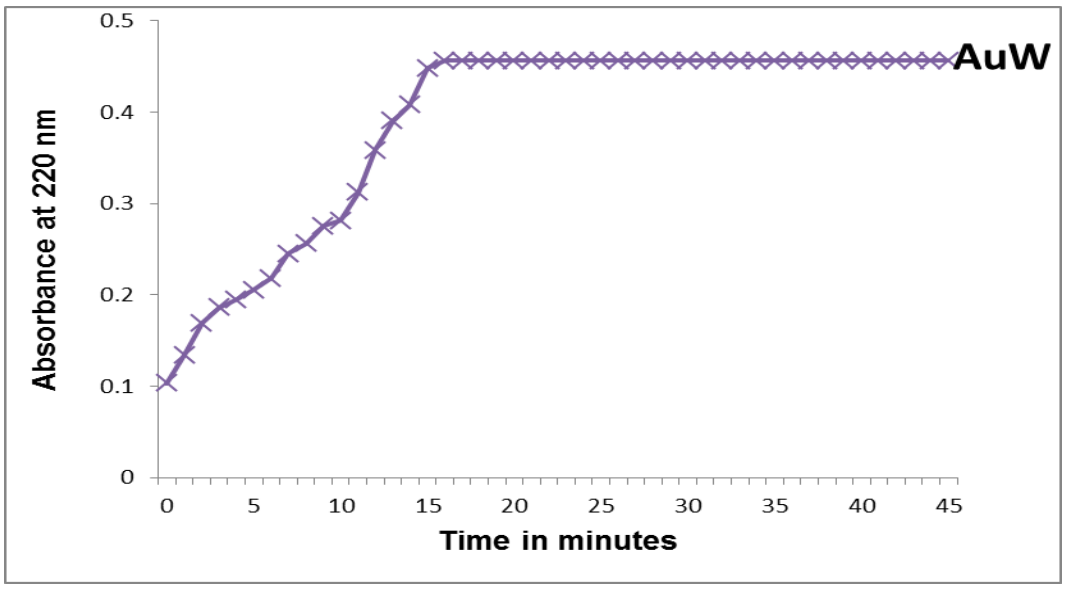

Ram *et* al. (2013) studied the *in vitro* release of silver nanoparticles conjugated with azathioprine and showed that two third of the drug released with 24 hours. Gnaeshkumar and Poornachandra (2015) reported the release of miconazole from its silver nanoparticles to be higher at acidic pH.

In the present study, the effect of silver and gold nanobioconjugates synthesized from *C. ternatea* also showed slow release. The results of *in vitro* antibacterial and *in vivo* anti-inflammatory assays showed that the extent of antibacterial and anti-inflammatory activities rendered by the nanoparticles were better than their methanolic leaf extratcs. The nanobioconjugates were also found to be biocombatible, indicating their safety.

Thus, our results show that the nanobioconjugates can safely be adminsitered to humans to achieve enhanced bioefficacy against bacterial pathogens and inflammation.

PHASE IV:

Phase IV, the final phase of the study, involved the *in vivo* analysis of anti-inflammatory activity of leaf extracts to validate the *in vitro* results obtained.

4.7 ASSESSMENT OF *in vivo* ANTI-INFLAMMATORY ACTIVITY OF METHANOLIC LEAF EXTRACTS AND THEIR NANOBIOCONJUGATES IN ANIMAL MODEL:

In vivo assessment in experimental animals provide the most physiologically relavent test system and gives information that relates the effects observed under *in vitro* conditions (Tingle and Helsby, 2006). In the present study, the methanolic leaf extracts and their nanobioconjugates were evaluated for *in vivo* anti-inflammatory activity against acute and chronic inflammation, in animal model.

4.7.1 Assessment of *in vivo* anti-inflammatory activity against acute inflammation:

The initial phase of edema formation is attributed to the release of histamine and serotonin. The second phase of edema is due to the release of prostaglandins, protease and lysosomal contents. Subcutaneous injection of carrageenan into the rat paw produces inflammation resulting from plasma extravasation, increased tissue water and plasma protein exudation along with neutrophil extravasation, all due to the metabolism of arachidonic acid. The first phase begins immediately after injection of carrageenan and diminishes in two hours. The second phase begins at the end of first phase and remains through third hour up to five hours (Nile and Park, 2013). Carrageenan injection induced edema and reached a maximum value at three hours. It decreased slowly within 6 hours and further decreased in 48 hours. Both the leaf extracts and their silver and gold nanobioconjugates significantly reduced the edema formation in the first phase (till 3rd hours) as well as in the second phase (from 4th hours onwards) of inflammation, as shown in Figure

4.33. Plate 4.9 shows the paw edema induced by carrageenan in control mice.

Figure 4.33

Anti-inflammatory activity of methanolic extracts of *Clitoria ternatea* leaves bearing blue and white flowers and their silver and gold nanobioconjugates on carrageenan induced paw edema in mice

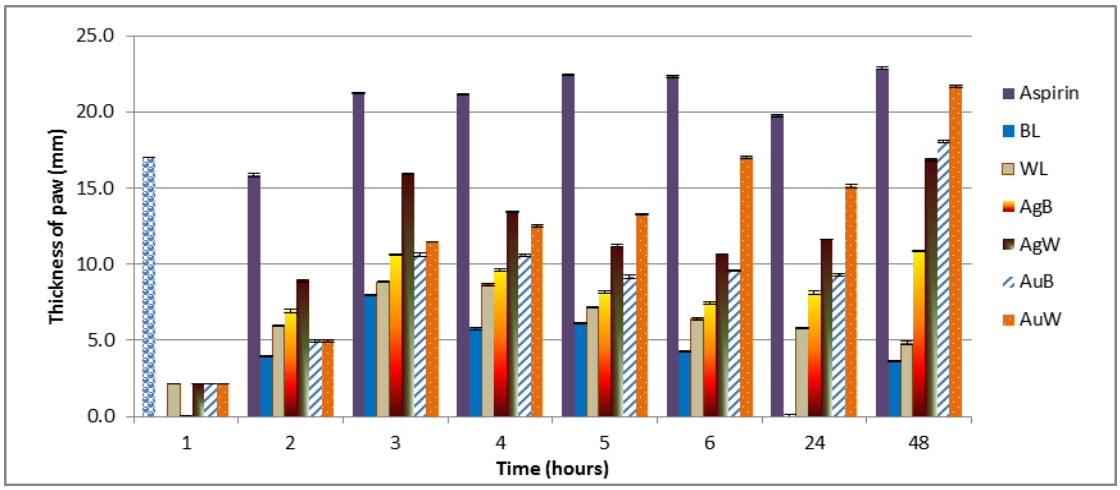

The values are mean ± SD, n=5
BL- blue leaf extracts; WL- white leaf extracts;
AgB- silver nanobioconjugates from blue variety;
AgW- silver nanobioconjugates from white variety;
AuB- gold nanobioconjugates from blue variety;
AuW- gold nanobioconjugates from white variety

Plate 4.9

Mice with carrageenan-induced paw edema

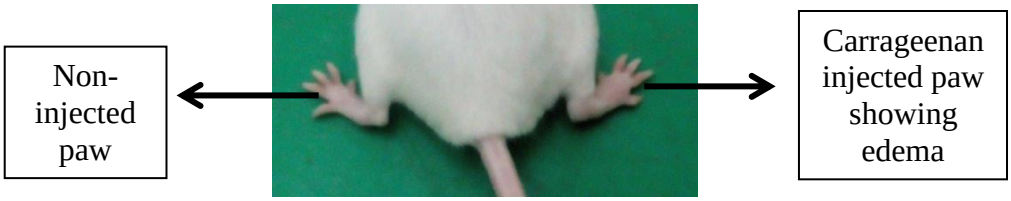

Wang *et al*. (2016) discovered bioactive compounds from the aerial parts of *A. frigida* and reported their anti-inflammatory effects against inflammation induced by carrageenan and egg albumin in rats. Shah and Patel (2015) studied the anti-inflammatory activity of the polymeric NPs loaded gel on carrageenan induced paw edema model in the experimental

animal system, Albino Wistar rats and observed maximum inflammation after 2 hours of injection, increase in % inhibition of paw-edema was seen up to 6 hours and 10 hours.

Ma *et al*. (2013) studied the anti-Inflammatory effects of 4-methylcyclopentadecanone on xylene-induced mouse ear edema and carrageenan-induced mouse paw edema in mice. The results showed a remarkable inhibition. Chouaib *et al*. (2015) reported that the oleanolic acid derivatives display anti-inflammatory activity. Sarkhel (2015) reported the anti-inflammatory activities of the aqueous extract of commercially partially purified saponin from *Quillaja saponaria* Mol. in *in vivo* animal models using carrageenan induced mice paw edema.

David *et al*. (2014) evaluated the anti-inflammatory effects of AgNPs from European black elderberry fruit extracts *in vivo* on acute inflammation model and in humans on psoriasis lesions and found that the pre-administration of AgNPs reduced the edema and cytokines levels in the paw tissues, early after the induction of inflammation demonstrating the possible use of synthesized AgNPs for the treatment of psoriasis lesions. Cheng *et al*. (2014) studied the ethanol extract and its derived fractions of *Pyrrosia petiolosa* obtained with solvents of different polarities for anti-inflammatory activity using the mouse ear swelling induced by xylene.

Uchiyama *et al*. (2014) studied the anti-inflammatory properties of gold nanoparticle bioconjugates and found that the bioconjugates did not cause lysis of human erythrocytes, apoptosis or necrosis of human leukocytes, and endothelial cells *in vitro*, thus confirming their anti-inflammatory effects *in vitro*. Joseph *et al*. (2013) evaluated the anti-inflammatory activity of various extracts of fresh leaves of *Clerodendrum paniculatum* Linn. by *in vitro* (human red blood cell membrane stabilization method) and *in vivo* methods (carrageenan-induced rat paw edema method).

Faujdar *et al*. (2016) evaluated the anti-inflammatory activity of hydroalcoholic extracts of bark and leaves of *Acacia ferruginea* DC. by carrageenan-induced paw edema method an reported that the extracts inhibited the inflammation as comparable to indomethacin. Lee *et al*. (2016) studied the potential anti-inflammation activity and depigmentation effect of Lespedeza bicolor extract and its fractions and found that that *L. bicolor* extract have anti-inflammatory, antioxidant activities and tyrosinase inhibitory effect. Donalda *et al*. (2016) analysed anti-inflammatory activity of *Aleurites moluccanus* extract using an *in vivo* paw edema model and reported that the dried extract inhibited paw edema.

Our results of acute paw edema in mice model also proved that the silver and gold nanobioconjugates of *C. ternatea* leaves are potential source of anti-inflammatory drugs.

4.7.2 Assessment of *in vivo* anti-inflammatory activity against chronic inflammation:

Adjuvant-induced arthritis method was used to assess the *in vivo* anti-inflammatory activity of methanolic extracts of *Clitoria ternatea* leaves bearing blue and white flowers and their silver and gold nanobioconjugates against chronic inflammation in mice model. The paw thickness was recorded on the day of injection and on day 5. To assess the severity of the induced adjuvant disease, the non-injected paw (secondary lesions) thickness was recorded and the body weight were determined again on the day 21. The polyarthritis severity was also graded. The results are presented below.

There was a slight weight difference in the test groups (plant extracts or nanobioconjugates) and standard group (aspirin). The maximum weight loss was recorded in the control group, where the animals induced with FCA without any treatment (aspirin or plant extracts or nanobioconjugates) presented in the Figure 4.34.

Figure 4.34

Weight difference due to anti-inflammatory activity on adjuvant-induced arthritis in mice by *C. ternatea* leaf extracts and their silver and gold nanobioconjugates

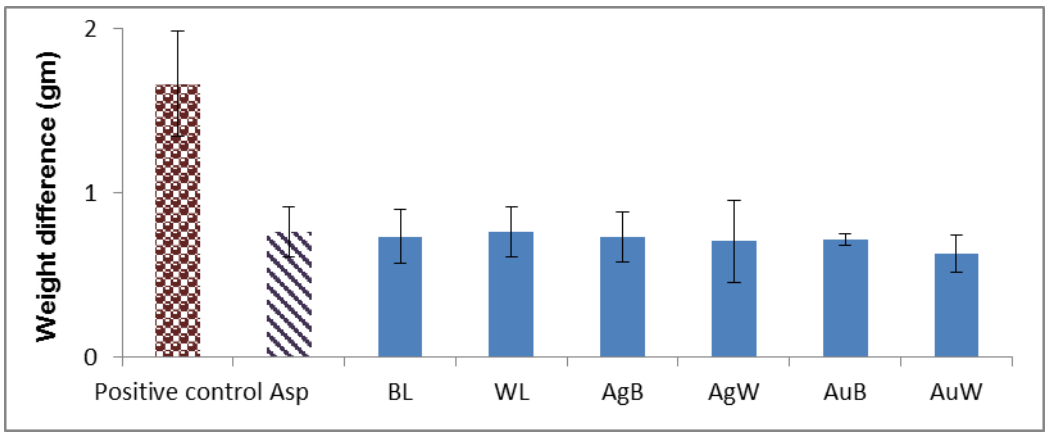

In primary lesions, standard (aspirin) showed maximum inhibition and all the NPs showed inhibition compared with control (Plate 4.10). The effects of test samples were significantly less than that of standard. Gold nanobioconjugates significantly inhibited the primary lesion followed by silver nanobioconjugates. The white variety showed better inhibition compared to blue variety (Figure 4.35).

Plate 4.10

Mice with primary lesion (Day 5)

Figure 4.35

Effect of methanolic extracts of *Clitoria ternatea* leaves bearing blue and white flowers and their silver and gold nanobioconjugates on primary lesions due to anti-inflammatory activity on adjuvant-induced arthritis in mice

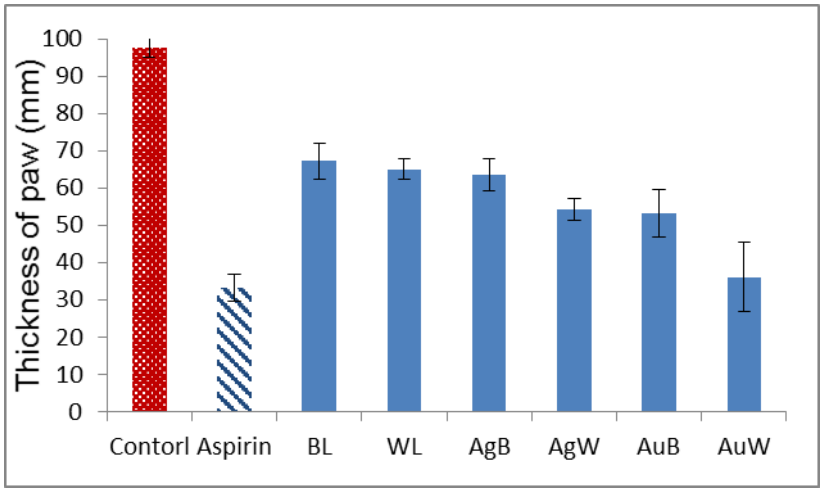

In the secondary lesions also (Figure 4. 36) standard (aspirin) showed maximum inhibition compared with control (Plate 4.11). All the test samples showed better inhibition compared with control. The effects of nanobioconjugates were comparable with that of standard. Gold nanobioconjugates significantly inhibited the secondary lesion followed by silver nanobioconjugates. White variety showed better inhibition compared to blue variety.

Plate 4.11

Mice with secondary lesion (Day 21)

Figure 4.36

Effect of methanolic extracts of *Clitoria ternatea* leaves bearing blue and white flowers and their silver and gold nanobioconjugates on secondary lesions due to anti-inflammatory activity on adjuvant-induced arthritis in mice

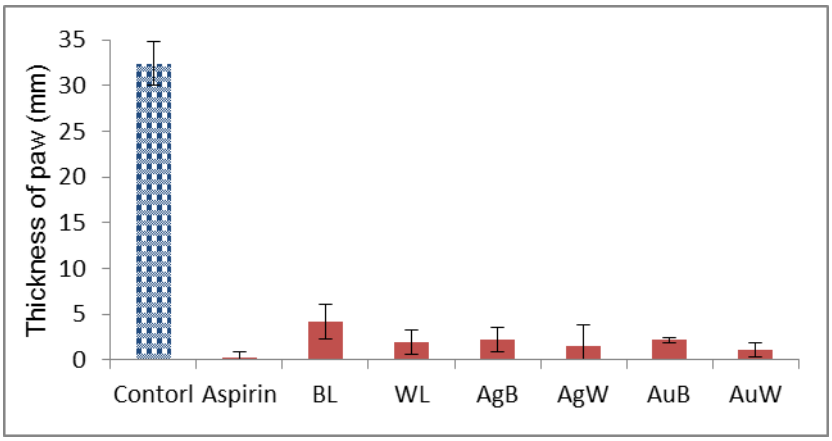

The highest arthritis index was recorded in the control group and the lowest in the aspirin (Figure 4.37). The test groups and the standard drug treated group significantly decreased the arthritis index in the adjuvant-induced arthritis mice as compared with the control group. Plate 4.12 shows arthritis in control mice.

Plate 4.12

Mice with arthritis (Day 21)

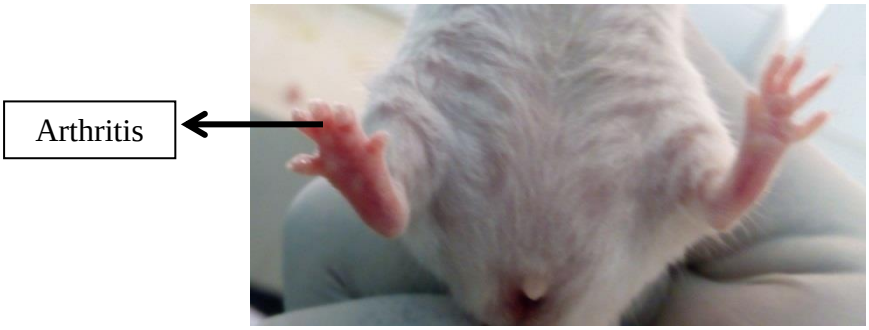

From the results, it is clear that the nanobioconjugates were better than the unconjugated plants extracts in terms of chronic anti-inflammatory activity from the three parameters analyzed, namely, primary lesion, secondary lesion

and arthritis index. The gold nanobioconjugates were better than the silver nanobioconjugates and, among the two varieties tested, the white variety showed better inhibitory activity than blue variety of the plant *C. ternatea.*

Figure 4.37

Effect of methanolic extracts of *Clitoria ternatea* leaves bearing blue and white flowers and their silver and gold nanobioconjugates on arthritis index due to anti-inflammatory activity on adjuvant-induced arthritis in mice

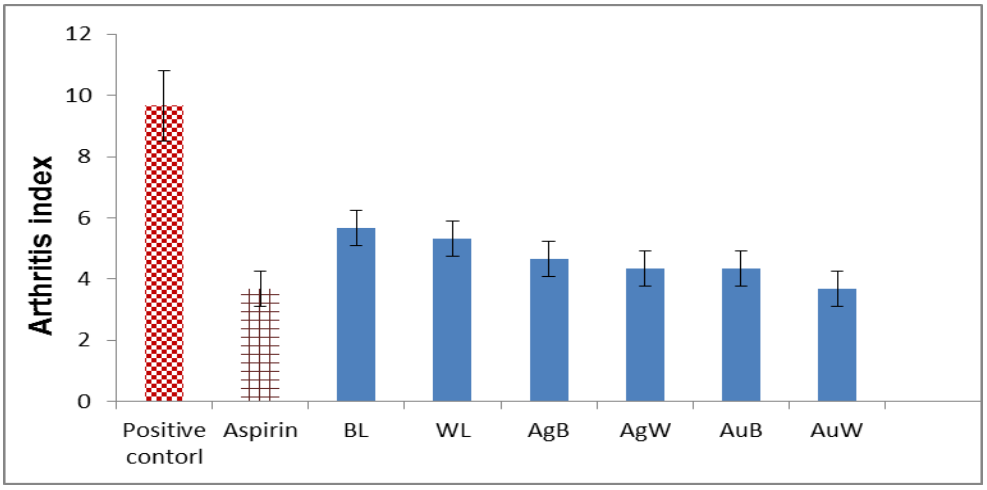

The values are mean ± SD, n=5
BL- blue leaf extracts; WL- white leaf extracts;
AgB- silver nanobioconjugates from blue variety;
AgW- silver nanobioconjugates from white variety;
AuB- gold nanobioconjugates from blue variety;
AuW- gold nanobioconjugates from white variety

Shaikh *et al*. (2015) evaluated the anti-inflammatory activity of selected medicinal plants used in Indian traditional system of medicine *in vitro* as well as *in vivo* and reported that the selected plants can be considered as a resource for searching novel anti-inflammatory agents. Singh *et al*. (2016) evaluated the *in vivo* anti-inflammatory potential of stem bark extract of *Dillenia indica* f. elongata (Miq.) in comparison with *Shorea robusta* Gaertn. in experimental animals and reported that the ethyl acetate extracts of *D. indica* f. *elongata* and *S. robusta* possessed good central as well as peripheral analgesic activity as compared with pentazocine and indomethacin

respectively in both acute (carrageenan-induced) and chronic (formalin-induced) models of inflammation.

Filhoa *et al*. (2016) reported the anti-inflammatory effect of curcuminoids from *Curcuma longa* L. in reduced intestinal mucositis induced by 5-fluorouracil in mice. Husain *et al*. (2016) investigated the imidazolidine derivatives (3a-k) for their anti-inflammatory activity in Wistar albino rats and reported three derivatives possessing promising anti-inflammatory effect. Cheng *et al*. (2015) evaluated the anti-inflammatory effects of Guge Fengtong formula using *in vivo* animal models and reported that the extracts significantly attenuated ear edema, decreased carrageenan-induced paw edema, reduced the arthritis score, and reversed the weight loss of the complete Freund's adjuvant-injected rats.

In our results also the nanobioconjugates reduced carrageenan-induced paw edema, reduced the arthritis score, and reversed the weight loss of the complete Freund's adjuvant-injected mice proving their potential as anti-inflammatory drugs.

The present study demonstrated that the methanolic extract of the *Clitoria ternatea* leaves showed significant anti-inflammatory activity against acute and chronic inflammation. The *in vivo* study results confirmed the results obtained in the *in vitro* studies, which validate the results obtained *in vitro*. The results clearly prove that the leaves of *Clitoria ternatea* are potential source of anti-inflammatory drugs. The study also proves that the synthesis of nanobioconjugates improves the bioactivity of the plant extract. Gold nanobioconjugates were better than silver nanobioconjugates and the white variety was better than the blue variety. Further studies are required to establish and elaborate the molecular mechanism for proper clinical utility.

The results obtained are summarized and conclusions drawn therein are presented in the next chapter.